https://doi.org/10.5194/gmd-2023-217
Preprint. Discussion started: 4 January 2024

Geoscientific Model Development Discussions

Improving subseasonal forecast skill in the Norwegian Climate Prediction Model using soil moisture data assimilation

Akhilesh S. Nair[1], François Counillon[1,2], and Noel Keenlyside[1]

[1]Geophysical Institute, University of Bergen, and Bjerknes Centre for Climate Research, Bergen, Norway
[2]Nansen Environmental and Remote Sensing Center, and Bjerknes Centre for Climate Research, Bergen, Norway

Correspondence: Akhilesh Nair (akhilesh.nair@uib.no)

Abstract. This study emphasises the importance of soil moisture (SM) in subseasonal-to-seasonal (S2S) predictions at mid-latitudes. To address this we introduce the Norwegian Climate Prediction Model Land (NorCPM-Land), a land reanalysis framework tailored for integration with the Norwegian Climate Prediction Model (NorCPM). NorCPM-Land assimilates blended SM data from the European Space Agency's Climate Change Initiative into a 30-member offline simulation of the Community Land Model with fluxes from the coupled model. The assimilation of SM data reduces error in SM by 10.5 % when validated against independent SM observations. It also improves latent heat flux estimates, illustrating that the adjustment of underlying SM significantly augments the capacity to model land surface dynamics. We evaluate the added value of land initialisation for subseasonal predictions, by comparing the performance of hindcasts (retrospective prediction) using the standard NorCPM with a version where the land initial condition is taken from NorCPM-Land reanalysis. The hindcast covers the period 2000 to 2019 with four start dates per year. Land initialisation improves predictions up to a 3.5-month lead time for SM and a 1.5-month lead time for temperature and precipitation. The largest improvements are observed in regions with significant land-atmospheric coupling, such as the Central United States, the Sahel, and Central India. It also better captures extreme (high and low) temperature events in parts of Europe, the United States, and Asia, at mid and high latitudes. Overall, our study provides further evidence for the significant role of SM content in enhancing the accuracy of subseasonal predictions. This study provides an technique for improved land initialisation, utilising the same model employed in climate predictions.

1 Introduction

Subseasonal-to-seasonal (S2S) forecasts have significant societal implications, especially in the water resources management, agribusiness, and emergency response sectors (Merryfield et al., 2020). There is, however, a considerable gap in accurate prediction at S2S range because of the chaotic processes affecting the sources of predictability (Meehl et al., 2021; Mariotti et al., 2018). It is essential to understand the sources of S2S predictability better and develop more accurate monitoring and prediction systems. The land surface is an important factor in determining the predictability and variability of the climate at S2S timescales (Koster et al., 2004; Guo et al., 2011) – up to 4-week lead time (Mariotti et al., 2018). In regions where there is substantial land-atmosphere coupling, soil moisture (SM) exerts a direct influence on the atmosphere. It influences latent and sensible heat fluxes and thus regulates the land-atmosphere feedbacks (Koster et al., 2004; Dirmeyer and Halder, 2016). SM

https://doi.org/10.5194/gmd-2023-217
Preprint. Discussion started: 4 January 2024


Geoscientific Model Development Discussions

can also influence hydro-meteorological factors such as temperature and precipitation (Koster et al., 2004; Seneviratne et al., 2010; Taylor et al., 2012a). Previous studies have shown that SM affects the accuracy of seasonal predictions (Fischer et al., 2007; Koster et al., 2010; Dirmeyer and Halder, 2016; Dirmeyer et al., 2018; Seo et al., 2019, 2020). The persistence of SM anomalies over time (also known as SM memory) is longer than for meteorological variables, hence enhancing subseasonal forecasts (Orth and Seneviratne, 2012; McColl et al., 2017; Santanello Jr et al., 2018).

The Norwegian Climate Prediction Model (NorCPM) provide climate reanalyses (Counillon et al., 2016) and seasonal-to-decadal climate predictions (Counillon et al., 2014; Bethke et al., 2021; Hermanson et al., 2022). The model is used to perform monthly operational S2S predictions, which are provided to stakeholders through the Norwegian center for research innovation Climate Futures (https://klimavarsling.no). The current data assimilation (DA) scheme is not ideal for such applications: it only updates the ocean and sea ice components (Kimmritz et al., 2019; Bethke et al., 2021); while the atmosphere and land components are only weakly constrained to observations through their dynamical adjustment to the ocean and sea-ice states (which are updated by the assimilation).

This study aims to enhance land surface initialisation within NorCPM and to examine the impact of the improved land initialisation on S2S prediction skill. Data from existing land reanalysis can be used directly as initial conditions for land surface components (e.g., Li et al., 2019), but discrepancies in the models, resolutions and grids tend to generate dynamical imbalances and drift during the predictions (Pohlmann et al., 2009). Here, we aim to constrain the land component of the same model used for running predictions, by performing our own land reanalysis—hereafter called NorCPM-Land. Subsequently, we assess the benefits of SM initialisation for S2S prediction by comparing the hindcast skill of the standard NorCPM with a version where the land initial state is from NorCPM-Land.

The community land model (CLM) used in NorCPM simulates key land surface processes (Oleson et al., 2010) and provides SM estimates at different soil depths down in the vadose zone. Uncertainty in the land state grows inherently with errors in the atmospheric forcing and inaccuracy in the land surface processes. Data assimilation (DA) of SM can constrain such error (Kumar et al., 2012; Nair and Indu, 2019; Reichle and Koster, 2004). In-situ SM observations are too sparse and heterogeneously distributed to constrain the land surface model effectively, but SM measurements can be derived from passive and active microwave satellite remote sensing. We rely here on the daily SM from the European Space Agency's Climate Change Initiative (ESA CCI; Gruber et al., 2019) to update CLM states. ESA CCI provides a consistent SM product from the multi-satellite products.

While direct online assimilation of SM data into NorCPM would be preferable, NorCPM is currently working offline – meaning that the model is stopped, the state is written on disk, DA is applied to the files, and the model restarted. The time required for initialising the model and writing the input/output is burdensome (Karspeck et al., 2018), and the required daily frequency for SM assimilation is not feasible with our current NorCPM configuration. To address this limitation, NorCPM-Land performs daily offline assimilation of SM data. This is accomplished by utilising CLM with identical version and resolution settings as those employed in NorCPM. The atmospheric ensemble flux, consisting of 30 members, for the offline CLM is sourced from a historical ensemble of simulations generated by the earth system model utilised in NorCPM.

https://doi.org/10.5194/gmd-2023-217
Preprint. Discussion started: 4 January 2024


Geoscientific Model Development Discussions

The NorCPM-Land relies on EnKF (Evensen, 2003) that is a flow-dependent assimilation method, and which has proven successful for land DA (Reichle and Koster, 2004; Drusch et al., 2009; De Rosnay et al., 2013; Kumar et al., 2012; Nair and Indu, 2016, 2019; Nair et al., 2022; Pradhan et al., 2023). During the assimilation process, we use a cumulative density function matching approach to ensure that DA does not alter the distribution of the quantity assimilated. Our assimilation framework ensures that the model's climatology remains unchanged – in good agreement with the initialisation of the other component in NorCPM – thereby minimising hindcast drift.

To assess the influence of the land component on the resultant prediction skill, we conducted a comparison between two sets of sub-seasonal hindcasts (retrospective predictions). One set utilised the standard NorCPM, while the other incorporated land initial conditions derived from NorCPM-Land reanalysis. This hindcast study spanned from 2000 to 2019, featuring four different start dates per year and comprising 30 members for each hindcast. Notably, it did not necessitate the application of drift correction. The integration of land initialisation led to a notable enhancement in SM predictions, extending up to 3.5 lead months, as well as improvements in surface temperature and precipitation predictions, extending up to 1.5 lead months. We discuss potential avenues to refine our approach and further improve the accuracy and reliability of our initialisation approach.

2 Model description

2.1 Norwegian Earth System Model

The NorCPM is based on the Norwegian Earth System Model (NorESM). We use here the NorESM1-ME (Bentsen et al., 2013; Tjiputra et al., 2012). NorESM1 is based on the Community Earth System Model version 1.0.3 (CESM1; Hurrell et al., 2013), but differs in the ocean component, atmospheric chemistry, and ocean biogeochemistry. The land component is the CLM version 4 (Oleson et al., 2010). The ocean component of NorESM is an upgraded version of the isopycnal coordinate ocean model MICOM (Bleck et al., 1992), referred to as Bergen Layered Ocean Model (Bentsen et al., 2013). The ocean biogeochemistry is based on the Hamburg Ocean Carbon Cycle Model (HAMOCC, Assmann et al., 2010; Tjiputra et al., 2012). The sea ice component is a version of the Los Alamos Sea ice model (CICE4, Gent et al., 2011; Holland et al., 2012). The ocean and the sea-ice model have a horizontal resolution of approximately 1°. The atmosphere component is a version of the Community Atmosphere Model (CAM4-Oslo, Kirkevåg et al. 2013), which provides choices for aerosol and cloud chemistry (Kirkevåg et al., 2013). CAM4 has a horizontal resolution of 1.9° latitude and 2.5° longitude and 26 vertical levels in a hybrid sigma-pressure coordinate; CLM follows the same horizontal grid as CAM4.

2.2 Community Land Model

The CLM model is an integrated land model based on water and energy balance equations. Land surface in CLM follows a subgrid hierarchy, with each grid cell consisting of land units, columns, and plant functional types (PFTs). Grid cells can have different numbers of land units, like lakes, glaciers, vegetation, and urban areas. Each column in the vegetated land units has 15 layers of soil and 5 layers of snow, depending on the snow depth. The default configuration of the soil profile in CLM

https://doi.org/10.5194/gmd-2023-217
Preprint. Discussion started: 4 January 2024

Geoscientific Model Development Discussions

consists of 15 strata with thicknesses ranging from 17.5 mm, 45.1 mm, 90.6 mm, 165.5 mm, 289.1 mm, 492.9 mm, 828.9 mm, 1382.8 mm, 2296.1 mm, 3801.9 mm, 6284.5 mm, 10377.5 mm, 17125.9 mm, 28252.0 mm, 42103.2 mm in each active grid cell. The top 10 hydrologically active strata are used to compute the SM. To simulate changes in canopy water, surface water, snow water, soil water, soil ice, and water in the unconfined aquifer, the model parameterizes interception, throughfall, canopy drip, snow accumulation and melt, water transfer between snow layers, infiltration, evaporation, surface runoff, sub-surface drainage, redistribution within the soil column, and groundwater discharge and recharge. In CLM the multilayer vertical moisture and energy transfer in a one-dimensional soil model are predicted using a modified Richard's equation. Similarly, to derive the land surface fluxes, the similarity theory developed by Monin and Obukhov is adopted. CLM considers the spatial heterogeneity of the land surface, and it simulates the SM, soil temperature, infiltration, evapotranspiration, sensible heat flux, latent heat flux, and soil heat flux (Orth and Seneviratne, 2012). The soil hydraulic and thermal characteristics in CLM are derived from the pedotransfer functions of sand and clay (Cosby et al., 1984) and organic properties of the soil (Lawrence and Slater, 2008). In this work, the CLM is configured by incorporating the following components: DATM; CLM; SICE; SOCN; RTM; SGLC; SWAV. The resolution of the model is set to f19_g16 globally, with a total of 288 (longitude) 192 (latitude) grid cells.

2.3 Data assimilation: Ensemble Kalman Filter

The DA system is based on the Ensemble Kalman Filter (EnKF). The observations are sampling to the true model state ($\mathbf{x}^t$).

$$\mathbf{y} = \mathbf{H}\mathbf{x}^t + \epsilon, \tag{1}$$

where the $\mathbf{H}$ is the observation operator that project the model space to the observations space, $\mathbf{y}$ is the observation vector, and ϵ is the observation error that is assumed to be a Gaussian random error with zero mean and observation error covariance matrix $\mathbf{R}$. Similarly, the forecast ensemble $\mathbf{X}^f$ and the ensemble mean $\mathbf{x}^f$ are assumed to be unbiased, and the forecast error is approximated by the sample error covariance matrix $\mathbf{P}^f$, with $\mathbf{P}^f = \frac{1}{n-1}\mathbf{A}^f\mathbf{A}^{f\mathrm{T}}$, with n being the ensemble size, the ensemble anomaly $\mathbf{A} = \mathbf{X} - \mathbf{x}\mathbb{1}^{\mathrm{T}}$ and the $\mathbb{1}_n = [1, 1, ..., 1] \in \mathcal{R}^{1\times n}$

We update the ensemble mean as follows:

$$\mathbf{x}^a = \mathbf{x}^f + \mathbf{K}(\mathbf{y} - \mathbf{H}\mathbf{x}^f), \tag{2}$$

where $\mathbf{K}$ is the Kalman gain matrix, computed as follows:

$$\mathbf{K} = \mathbf{P}^f\mathbf{H}^{\mathrm{T}}(\mathbf{H}\mathbf{P}^f\mathbf{H}^{\mathrm{T}} + \mathbf{R})^{-1}. \tag{3}$$

The superscripts f and a denote the forecast and the analysis estimates.

We use the Ensemble Square Root Filter (EnSRF) that solves the analysis without perturbing observations and performs more optimally than the stochastic EnKF (Whitaker and Hamill, 2002). The ensemble anomaly is updated as follows:

https://doi.org/10.5194/gmd-2023-217
Preprint. Discussion started: 4 January 2024

Geoscientific Model Development Discussions

$$\mathbf{A}^a = \mathbf{A}^f + \alpha\mathbf{K}(-\mathbf{H}\mathbf{A}^f), \tag{4}$$

$$\text{with } \alpha = \left(1 + \sqrt{\frac{\mathbf{R}}{\mathbf{H}\mathbf{P}^f\mathbf{H}^{\mathrm{T}} + \mathbf{R}}}\right)^{-1}.$$

2.4 ESA CCI SM observations

Satellite missions with active microwave sensors detect the backscattered value from the surface, while passive microwave sensors estimate SM from the surface emitted brightness temperature. Njoku et al. (2003) found that soil microwave emission originates from the top surface layer, with the emitting depth regulated by the dielectric properties of the near-surface moisture profile and decreasing with higher frequencies and wetter soils. The emission depth at C-band is about 1 cm or less, while at L-band it is roughly 2-5 cm (Ulaby et al. 1986). Some of the widely used missions for SM estimates are the Advanced Scatterometer (ASCAT) aboard the Meteorological Operational (METOP) satellites (Wagner et al., 2013), multi-frequency polarimetric microwave radiometer WindSat aboard the Coriolis satellite (Gaiser et al., 2004), and the Advanced Microwave Scanning Radiometer Earth Observing System (AMSR-E; Njoku et al. 2003) aboard Aqua satellite, among others, provide widely used satellite SM products. The Soil Moisture Ocean Salinity (SMOS) mission (Kerr et al. 2010) and Soil Moisture Active Passive (SMAP) mission (Entekhabi et al. 2010) also offer SM products. The European Space Agency's Climate Change Initiative (ESA CCI) provides a consistent SM product from the multi-satellite products. The ESA CCI SM v 06.1 is assimilated in this study. It incorporates over four decades of scatterometer-based active and radiometer-based passive microwave sensors from several satellite platforms. Datasets based on active sensors stem from the C-band (5.3 GHz) Active Microwave Instrument Wind Scatterometer (AMI-WS ERS-1/2 SCAT, 1991–2006; AMI-WS ERS-2, 1997–2007), Advanced Scatterometer (ASCAT), MetOp-A (2007–19), and MetOp–B (2012–19). The passive sensors used to generate SM are from the C-band (6.6 GHz) Scanning Multichannel Microwave Radiometer (SMMR, 1979–1987), the K-band (19.3 GHz) Special Sensor Microwave Imager (SSM/I, 1987–2013), the X-band (10.7 GHz) Tropical Rainfall Measuring Mission (TRMM) Microwave Imager (TMI, 1998–2015), the X-band (10.7 GHz) FengYun-3B Microwave Radiation Imager (FY-3B/MWRI, 2011–2019), and the X-band (10.7 GHz) Global Precipitation Measurement (GPM, 2014–20). The Advanced Microwave Scanning Radiometer 2 (AMSR-2, 20012–2019), WindSat (2007–2012), and the Advanced Microwave Scanning Radiometer for Earth Observing System (AMSR-E, 2002–11) are three more passive platforms that measure in the X band and C band. The SM Active and Passive mission (SMAP, 2015–19) and SM and Ocean Salinity (SMOS, 2010–2019) are the other two passive sensors that measure in the L band (1.4 GHz). The ESA CCI SM algorithm offers three distinct SM products. These include SM estimates derived solely from satellites equipped with active sensors, SM estimates derived solely from satellites equipped with passive sensors, and a merged product that integrates and harmonises SM retrievals from both. In this study, we specifically utilise the combined SM product derived from passive sensors. The passive data set spans the entire duration of the study and offers a resolution that adequately meets our requirements.

https://doi.org/10.5194/gmd-2023-217
Preprint. Discussion started: 4 January 2024

Geoscientific Model Development Discussions

2.5 NorCPM-Land reanalysis practical implementation

The production can be decomposed into two distinct stages (see the flowchart in Fig. 1): 1) producing the ensemble of atmospheric forcing required to run the offline CLM simulation and 2) assimilating SM daily into the offline ensemble of CLM to produce NorCPM-Land reanalysis. The ensemble of forcing is produced by running a 30-member ensemble of historical simulation of NorESM. We save precipitation, surface air temperature, humidity, pressure, and radiation forcing at 3 hourly intervals needed to run CLM offline for the period 2000–2019. The initial ensemble of NorESM is generated by sampling state from a stable preindustrial simulation and integrating it from 1850 to 2005 using CMIP5 historical forcings and with RCP8.5 scenario (Taylor et al., 2012b) from 2005-2019.

The reanalysis, as shown in Tab. 1, commences in January 1980 using the land initial conditions derived from the ensemble of NorESM historical simulations, referred to as FREE. We assimilate daily surface SM from ESA CCI. The assimilation only updates the SM of the first ten layers out of the 15 vertical layers that comprise the CLM state and does not update the other variables. In CLM, only the top 10 layers are considered hydrologically active, while the bottom 5 layers serve as thermal slabs and do not contribute to hydrological processes Lawrence et al. (2011).

Assimilation of SM occurs solely on land units defined as bare soil or vegetation. We do not assimilate in densely vegetated regions, due to the uncertainty in SM estimations from the ESA CCI (Sec. 2.4) in thick canopy cover and in regions covered by snow or frozen SM (Ulaby et al., 1987).

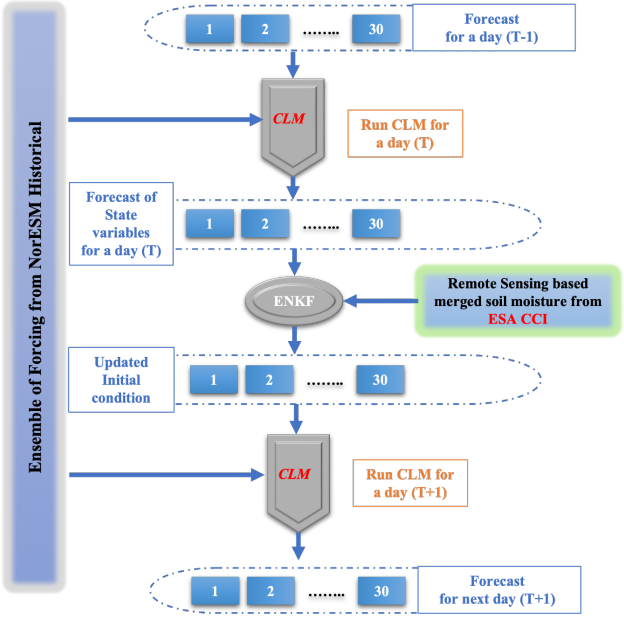

Figure 1. Flowchart of NorCPM-Land

https://doi.org/10.5194/gmd-2023-217
Preprint. Discussion started: 4 January 2024

Geoscientific Model Development Discussions

NorCPM uses an anomaly assimilation framework, meaning that the climatological monthly difference between the model and observations is removed before assimilation (Counillon et al., 2016; Bethke et al., 2021). For consistency, we developed a data assimilation of SM that does not change the climatological state of the land component. The bias between satellite and model-based SM estimates is large and is removed before the assimilation using the cumulative distribution function (CDF) mapping (Reichle and Koster, 2004; Kumar et al., 2012). A CDF matching is preferable to standard anomaly assimilation (Magnusson et al., 2013; Carrassi et al., 2014) for SM assimilation because the variable is non-Gaussian distributed. In this study, we employ a grid-point based simplified CDF rescaling approach similar to Scipal et al. (2008). However, we implemented a CDF mapping that is computed for each calendar month using the discrepancy between the ensemble mean of NorESM free run and ESA-CCI SM throughout the period 2000-2020. The monthly CDF matching approach removes seasonally dependent systematic bias between SM from model and observation. As such, **y** in Eq. 2 is replaced by a "bias corrected" observation, $SM_{\mathrm{CCI}}^{\mathrm{Bias\_corrected}}$ using Eq. 5.

$$SM_{\mathrm{CCI}}^{\mathrm{Bias\_corrected}} = \left(\overline{SM}_{\mathrm{NorESM}} - \left(\overline{SM}_{\mathrm{CCI}} \times \frac{\sigma_{\mathrm{NorESM}}}{\sigma_{\mathrm{CCI}}}\right)\right) + \left(\frac{\sigma_{\mathrm{NorESM}}}{\sigma_{\mathrm{CCI}}} \times SM_{\mathrm{CCI}}\right) \quad (5)$$

where $\overline{SM}_{NorESM}$ and $\overline{SM}_{CCI}$ are the daily mean SM of a particular month from NorESM and ESA CCI, respectively. Similarly, σ_{NorESM} and σ_{CCI} are the corresponding standard deviations. SM_{CCI} is the value of SM observation for a particular day. The CDF-matching is estimated for each calendar month and model grid point, and we show an example for two different months at a random location (Fig. 2). CDF matching considerably reduces the biases between ESA CCI data and NorESM (Fig. 2 a,b). Further, we rescale the observation error estimate from ESA CCI accordingly, to match with the bias-corrected observation in the DA.

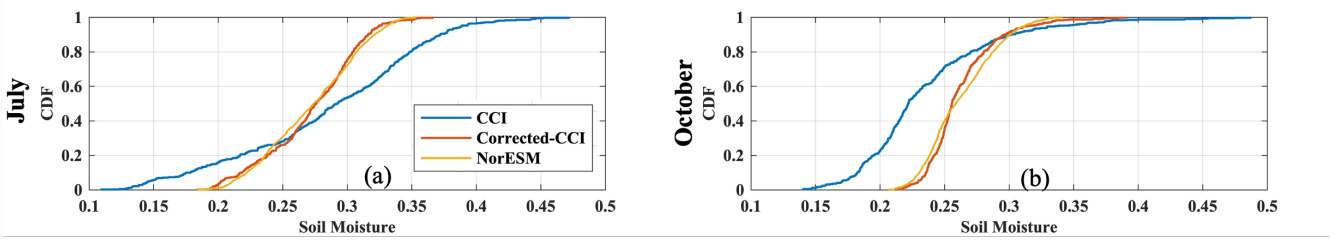

Figure 2. Example of CDFs from ESA CCI SM, NorESM (ensemble mean) along with ESA CCI after CDF matching for the calendar month of July and October at a location (selected randomly) near Central India – 25.58°N and Longitude 77.5°E.

Finally, we use a small multiplicative inflation (Anderson, 2001) of 1.05 (*i.e.,* 5 % inflation) to prevent a collapse of the ensemble spread. This was selected at the start of the experiment design, based on Ines et al. (2013).

2.5.1 Hindcast experiment setup

To assess the influence of land initialisation on predictions skill, we conduct two sets of sub-seasonal hindcasts (retrospective predictions) spanning 20 years from 2000 to 2019 (Tab. 1). The hindcast experiments are initiated quarterly on the 15th day

https://doi.org/10.5194/gmd-2023-217
Preprint. Discussion started: 4 January 2024

Geoscientific Model Development Discussions

of January, April, July, and October. The first set of hindcasts (Hind-S) is produced with the standard NorCPM prediction system (Wang et al., 2019; Bethke et al., 2021), in which the land component is not updated by assimilation – albeit some weak synchronisation can occur dynamically in between the monthly assimilation steps from the updated ocean and sea ice state. Initial conditions are taken from the 30 ensemble member NorCPM reanalyses. In the second set of hindcasts (Hind-S+L), the land component is replaced by that of NorCPM-Land reanalysis. Each hindcast comprises 30 realisations (ensemble members) and runs for 4 months. In total, there are 80 hindcasts (20 years with 4 hindcasts per year). The predictions use historical forcing from CMIP5 (Taylor et al., 2012a) up to 2005 and the representative Concentration Pathway 8.5 (RCP 8.5, Van Vuuren et al., 2011) afterwards. NorCPM assimilates monthly ocean observations in the middle of the month. As a consequence, the effective start of the hindcasts is after a half-month integration period. For example, a February hindcast assimilates January monthly averaged ocean data on the 15th of January. However, the primary objective is to quantify the additional benefits of land initialisation. SM data are only assimilated until the 15th of the month (until January 15th in the example above), and the subsequent days within the month will be referred to as lead month LM0.5 (second half of January in the example). For simplicity, we will subsequently denote the following predictions as LM1.5, LM2.5, and LM3.5 (being February, March and April in the given example).

Table 1. List of experiments.

Experiment Name	**Model**	**Run type**	**Assimilated observations in model components**		**Time Period**
			Land	**Other components**	
FREE	NorESM	Historical	×	×	1980-2019
NorCPM-Land	CLM 4 (offline)	Reanalysis	daily SM	×	1980-2019
NorCPM*	NorESM	Reanalysis	×	SST,T/S Profile	1980-2019
			Reanalysis used for initialisation		
			Land	**Other components**	
Hind-S	NorESM	Hindcast	NorCPM	NorCPM	2000-2019
Hind-S+L	NorESM	Hindcast	NorCPM-Land	NorCPM	2000-2019

*Configuration for NorCPM is based on Bethke et al. (2021) i2 version.

× Indicates that no observations are assimilated

3 Reference data sets

3.1 In Situ measurements

We use in-situ SM observations from the International SM Network for continental domain validation (ISMN; Dorigo et al., 2011) as the primary source of independent SM validation. We concentrate on locations with dense observational cover-

https://doi.org/10.5194/gmd-2023-217
Preprint. Discussion started: 4 January 2024


Geoscientific Model Development Discussions

age. Over the contiguous United States (CONUS), we use the Atmospheric Radiation Measurement (ARM), the FLUXNET-AMERIFLUX, the Cosmic-Ray Soil Moisture Observing System (COSMOS; Zreda et al., 2012), the Plate Boundary Observatory (PBO H2O; Larson et al., 2008), the Soil Climate Analysis Network (SCAN; Schaefer et al., 2007), the Snowpack Telemetry (SNOTEL). For validation over Europe, we use the (FR_Aqui Al-Yaari et al., 2018), Danish Hydrological Observatory and Exploratorium (HOBE; Jensen and Refsgaard, 2018), ORACLE, ((REMEDHUS, González-Zamora et al., 2019), the Norwegian water resources and energy directorate (NVE), the Finnish network (FMI, Ikonen et al., 2018). For validation over Asia, we use the central Tibetan Plateau (CTP_SMTMN, Yang et al., 2013) 2013), (MAQU, Dente et al., 2012) networks are used. For validation over Australia, we use the observations from the OzNet hydrological monitoring network (Young et al., 2008; Smith et al., 2012). This study further includes only hourly readings to a depth between 5 cm to 10 cm that are classified as "excellent quality" and concurrently measured for validation purposes. The daily mean SM is calculated after filtering the hourly data. Only locations with more than thirty per cent measurements during the study period are used for validation.

3.2 ERA5 and ERA5-Land

ERA5 (Hersbach et al., 2020) is the 5th global atmospheric reanalysis product from the European Centre for Medium-Range Weather Forecasts (ECMWF) available at a horizontal resolution of 0.25° and hourly frequency from 1940 to the present. It assimilates a large number of observations with the 4Dvar data assimilation method (Talagrand, 2014) —from around 0.75 million per day in 1979 to nearly 24 million per day by the end of 2018. The atmospheric component of ERA5 assimilates in situ observations of surface (10 m) wind over oceans and 2 m humidity over land along with pressure over both land and oceans. It also assimilates upper-air wind, temperature, and humidity from radiosonde, dropsonde, aircraft, and satellite observations. The land component further assimilates observations such as, screen level temperatures using two-dimensional optimal interpolation (2D-OI), SM using a Simplified Extended Kalman Filter (SEKF; De Rosnay et al., 2013), and snow temperature using an OI. We use ERA5 for validating our hindcast skill for precipitation and 2 m temperature (T2M).

We validate SM quantities using the ERA5-land reanalysis (Muñoz-Sabater et al., 2021). ERA5-Land reanalysis is generated by forcing an offline LSM with the ERA5 atmospheric reanalysis. It is available at an hourly temporal resolution and a spatial resolution of 0.1°×0.1° from 1950 to the present at https://cds.climate.copernicus.eu. ERA5-Land is built around the ECMWF land surface model: the Carbon Hydrology-Tiled ECMWF Scheme for Surface Exchanges over Land (HTESSEL). Each land grid-box is subdivided into up to six fractions (or tiles): bare ground, low and high vegetation, intercepted water, shaded and exposed snow. Each fraction has features that define distinct heat and water fluxes utilised to solve an energy balance equation for the tile skin temperature. According to Muñoz-Sabater et al. (2021), ERA5-Land considers grids with more than 50 % of their area covered by glaciers to be glacier grids, assuming a constant snow depth of 10 m.

3.3 GLDAS

The Global Land Data Assimilation System (GLDAS) was collaboratively designed and developed by the National Aeronautics and Space Administration (NASA) Goddard Space Flight Center and the National Oceanic and Atmospheric Administration National Centers for Environmental Prediction. The primary goal of GLDAS is to create a series of global land surface states

https://doi.org/10.5194/gmd-2023-217
Preprint. Discussion started: 4 January 2024

Geoscientific Model Development Discussions

and flux-related datasets that exhibit excellent performance. GLDAS employs four Land Surface Models (LSMs), namely Noah (Chen et al., 1996), Catchment (CLSM; Koster et al., 2000), CLM (Dai et al., 2003), and Variable Infiltration Capacity (VIC; Liang et al., 1994), and incorporates numerous observation datasets and reanalysis products to assimilate products with pixel resolutions of 0.25° and 1°. For more detailed information about GLDAS, please refer to (Rodell et al., 2004). This study utilises GLDAS Version 2.1 SM products, which stems from the monthly 1° resolution CLSM. The dataset can be downloaded from https://disc.gsfc.nasa.gov/datasets?keywords=GLDAS.

4 Metrics for skill assessment

In order to quantify the accuracy of our system, we use the Root Mean Square Error (RMSE) and the anomaly correlation coefficient (ACC). The metric are calculated comparing the ensemble-mean and the reference datasets. Because the amplitude of the seasonal changes is large and predictable, we subtract the seasonal cycle (hereafter referred to as deseasoned variability) from the model estimate (FREE and NorCPM-Land) and the reference before computing the RMSE and ACC. This also ensure that the model bias is removed, and we refer to the metric as bias free RMSE (bfRMSE).

$$\text{bfRMSE} = \left[\frac{1}{n}\sum\left((X-\overline{X})-(Y-\overline{Y})\right)^2\right]^{\frac{1}{2}} \tag{6}$$

$$\text{ACC} = \frac{\sum(X-\overline{X})(Y-\overline{Y})}{\sqrt{\sum(X-\overline{X})^2\sum(Y-\overline{Y})^2}} \tag{7}$$

The term X represent the model estimate and Y the observed estimate, and $\overline{X}$, $\overline{Y}$ are the monthly climatology. Note that X and Y can be at daily frequency. Validation is carried over the 40 years study period from 1980 to 2019. The improvement in NorCPM-Land skill after DA is represented using the reduction of bfRMSE (RRMSE).

$$\text{RRMSE} = \frac{\text{bfRMSE}_{\text{NorCPM-Land}} - \text{bfRMSE}_{\text{FREE}}}{\text{bfRMSE}_{\text{FREE}}} \times 100 \tag{8}$$

We also investigate the reliability of NorCPM-Land. The reliability is the property of the ensemble of a system to estimate its uncertainty (Counillon et al., 2016; Rodwell et al., 2016). The bfRMSE is calculated here with imperfect observations and the total error is the quadratic sum of the observation error variance (σ_o^2) and the ensemble forecast error variance (σ_m^2). In a perfectly reliable system, bfRMSE should be equal to the Total Error. In the following, we use a reliability index, which divides bfRMSE by the total error.

$$\text{R.I.} = \frac{\text{bfRMSE}}{\sqrt{\sigma_o^2+\sigma_m^2}} \tag{9}$$

A reliability index of one implies that the spread is ideal (Fortin et al., 2014), whereas a value more than one suggests a too-narrow spread (under dispersive), and a value less than one indicates a wide ensemble (over dispersive).

https://doi.org/10.5194/gmd-2023-217
Preprint. Discussion started: 4 January 2024


Geoscientific Model Development Discussions

We also use the atmospheric coupling index (ACI; Müller et al., 2021). This index shows whether alterations to a surface flux variable can influence precipitation changes. The areas where the coupling between the land and the atmosphere is strongest are known as the land-atmosphere hot spots. The ACI is computed using latent heat flux (LHF, λE), and precipitation (P) as in Eq. 10

$$\mathrm{ACI} = \frac{cov(\lambda E, P)}{\sigma(\lambda E)} \tag{10}$$

where $cov(\lambda E, P)$ represents covariance between LHF and precipitation, while $\sigma(\lambda E)$ represents the standard deviation along the time space. The ACI indicates the areas where latent heat fluxes impact precipitation. The reference ACI is computed using ERA5 precipitation and LHF data. To evaluate the impact of SM assimilation, we computed ACI using the flux component from CLM simulations (FREE, NorCPM-Land), with precipitation data still provided by ERA5. This analysis highlights the synchronisation of heat flux and precipitation due to SM assimilation, providing a preliminary evaluation of the atmospheric coupling of the offline land system.

5 Results

We first verify the performance of NorCPM-Land reanalysis with assimilated SM observations, and independent observations of SM, and land atmospheric coupling. We then analyse the impact of SM assimilation on prediction skill of SM and atmospheric quantities.

5.1 NorCPM-Land reanalysis evaluation

5.1.1 Sanity check with assimilated observation

We first assess the efficiency of the SM assimilation by comparing bfRMSE in the assimilated experiment with that of FREE using the assimilated observations. As this data is assimilated, it is imposed that error is reduced, but it is a starting point for verifying the performance of a DA system. The analysis shows that the error in FREE (Fig. 3a) has been effectively reduced in NorCPM-Land (Fig. 3b). The performance is stable through the analysis period (not shown).

https://doi.org/10.5194/gmd-2023-217
Preprint. Discussion started: 4 January 2024

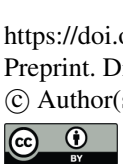

Geoscientific Model Development Discussions

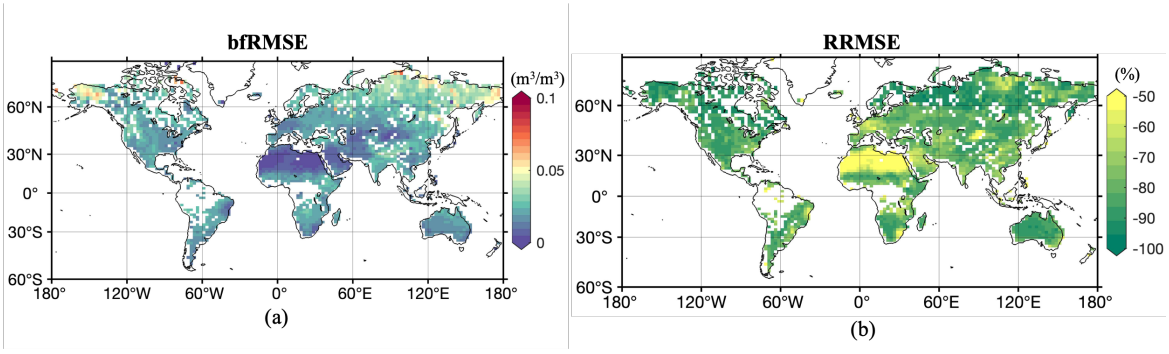

Figure 3. Depicts bfRMSE in FREE computed against ESA-CCI SM data (a), RRMSE (Eq. 8), in NorCPM-Land (b).

285 We then assess the reliability of the system – *i.e.,* R.I should be 1 in (Eq. 9). The reliability index is very small (global mean value of approximately 0.11), suggesting that the system is strongly over-dispersive (Fig. 4c). In the NorCPM-Land system, the reliability improves and achieves a global average of around 0.56 (Fig. 4d). This implies that the total error is now approximately twice the error of the ensemble mean.

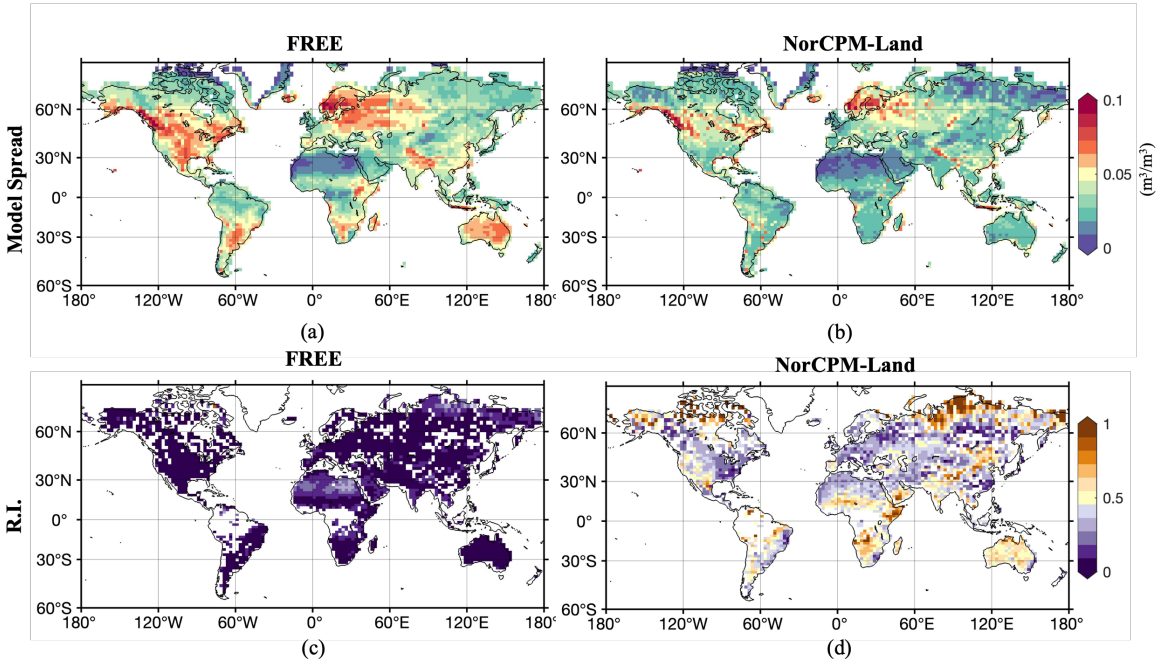

Figure 4. Depicts (a) the ensemble spread from FREE (b), from NorCPM-Land (c), the reliability index for FREE (d), and the reliability index for NorCPM-Land.

https://doi.org/10.5194/gmd-2023-217
Preprint. Discussion started: 4 January 2024

Geoscientific Model Development Discussions

5.1.2 Soil Moisture validation with independent data sets

The independent in situ observations from the International Soil Moisture Network (ISMN, Sec. 3.1) are used to validate the simulated daily averaged SM from NorCPM-Land. We compared the performance to that of FREE and of two widely-used land reanalysis products, namely ERA5-Land (Sec. 3.2) and GLDAS (Sec. 3.3).

In FREE, there is a significant error in SM over the western United States of America, parts of Europe, and Asia (Fig. 5a). These regions are of utmost importance for enhancing sub-seasonal forecasts due to their strong atmospheric coupling. In NorCPM-Land (Fig. 5b), bfRMSE is reduced globally by 10.5 % and by 25 % in specific regions such as parts of the USA and the Sahel, among others. The accuracy of NorCPM-Land reaches a comparable level of accuracy to ERA5-Land and GLDAS (Fig. 5c-e); reaching even lower bfRMSE than both reanalysis products. It is important to note that ERA5-Land and GLDAS do not explicitly assimilate SM (but only through using ERA5 to force ERA-Land, Sec. 3.2).

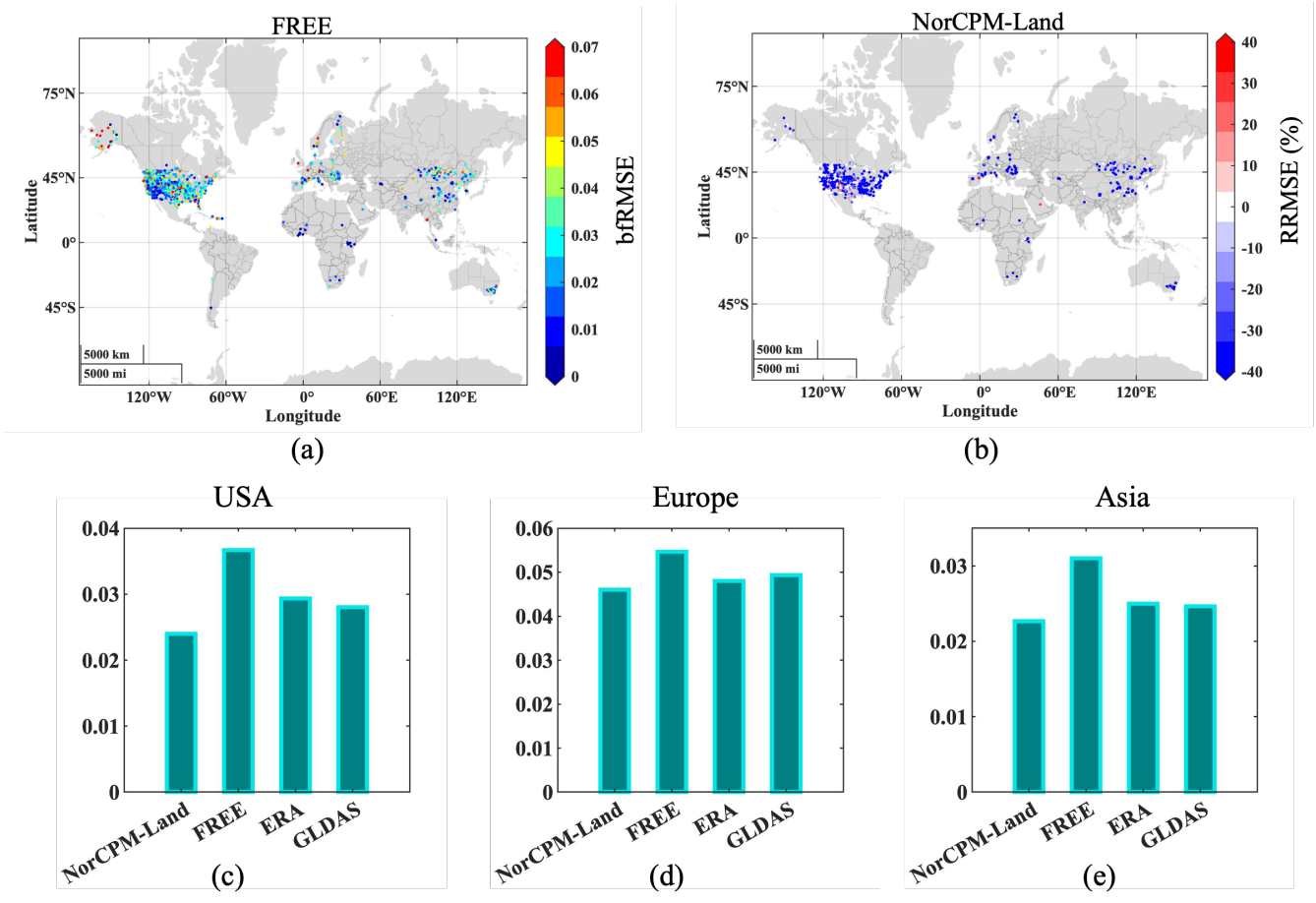

Figure 5. Daily average bfRMSE in FREE (a), RRMSE of NorCPM-Land (b) where cold color indicates regions with improvement, domain average of bfRMSE over USA (c), domain average of bfRMSE over Europe (d) , domain average of bfRMSE over Asia (e).

https://doi.org/10.5194/gmd-2023-217
Preprint. Discussion started: 4 January 2024

Geoscientific Model Development Discussions

However, the domain covered by in-situ measurements is relatively sparse. We pursue the evaluation of SM in NorCPM-Land by comparing it with existing reanalysis products, to asses skill in regions where in situ data is unavailable. We present here only the comparison with ERA5-Land for conciseness, but the results are comparable with GLDAS (not shown). NorCPM-Land significantly improves the SM simulation (Fig. 6) compared to FREE, particularly in arid regions such as the Sahara, Mexico, and Australia. The improvement is globally about 12.75%. The ACC in FREE (Fig. 6c) is relatively low (with a global average of 0.1), but reaches significant skill in regions where climate change have been most pronounced. The ACC in NorCPM-Land is higher (Figure 6d; 0.35 on global average). Regions of improvement coincide with region of reduced bfRMSE (*e.g.* in the Sahel region). Overall, this analysis confirms that SM assimilation in NorCPM-Land leads to improved variability of SM.

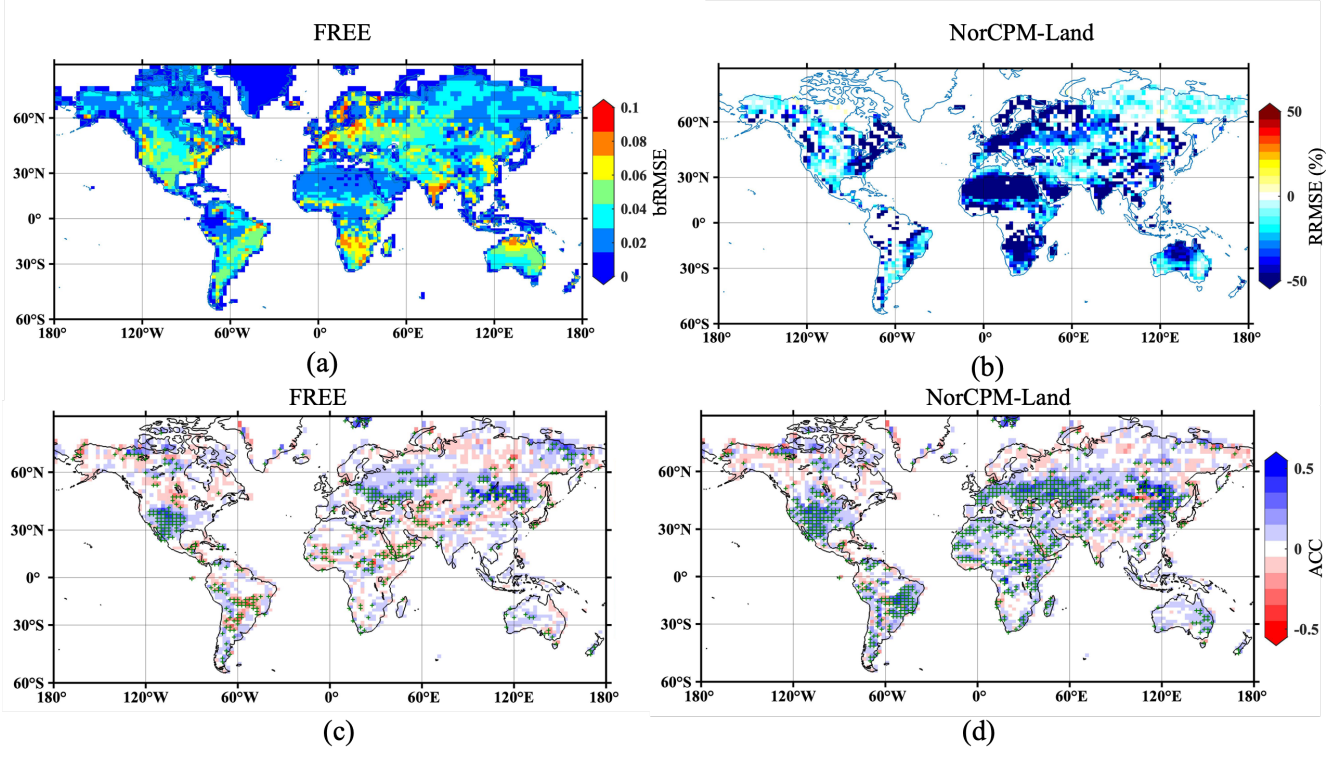

Figure 6. Pointwise bfRMSE of the monthly average of SM in FREE compared to ERA5-Land (a), RRMSE of NorCPM-Land (b). ACC of monthly averaged SM with respect to ERA5-Land in FREE (c) and NorCPM-Land (d). Cold colour indicates improvements (negative RRMSE and higher ACC). Grid-cells with significant correlation coefficient are marked with a green dot)

5.1.3 Improvement in Land-Atmospheric Coupling

The exchange of latent heat flux (LHF) between the land surface and the atmosphere plays a crucial role in the land-atmosphere energy transfer, as it directly affects evaporation and atmospheric moisture. The release of latent heat through precipitation leads to atmospheric drying, acting as a strong heating source. SM is one of the key variables influencing the latent heat flux.

https://doi.org/10.5194/gmd-2023-217
Preprint. Discussion started: 4 January 2024

Geoscientific Model Development Discussions

To assess the impact of SM assimilation on the land-atmosphere dynamics, we compare LHF of FREE and NorCPM-Land to that of ERA5-Land (Fig. 7). The improved SM estimates in NorCPM-Land yields a reduction of error of LHF compared to FREE. The global average RRMSE of NorCPM-Land is only -2.1 %, but the reduction is larger in regions with strong land-atmospheric coupling, such as parts of the Sahel and the USA, where RRMSE reaches up to -30 %. There are a few regions where the error in LHF is larger in NorCPM-Land than in FREE. However, it is important to note that performance of SM in NorCPM-Land regions with high LHF error was improved compared to FREE (Fig. 6), suggesting that the degradation relates to an atmospheric circulation bias in our model.

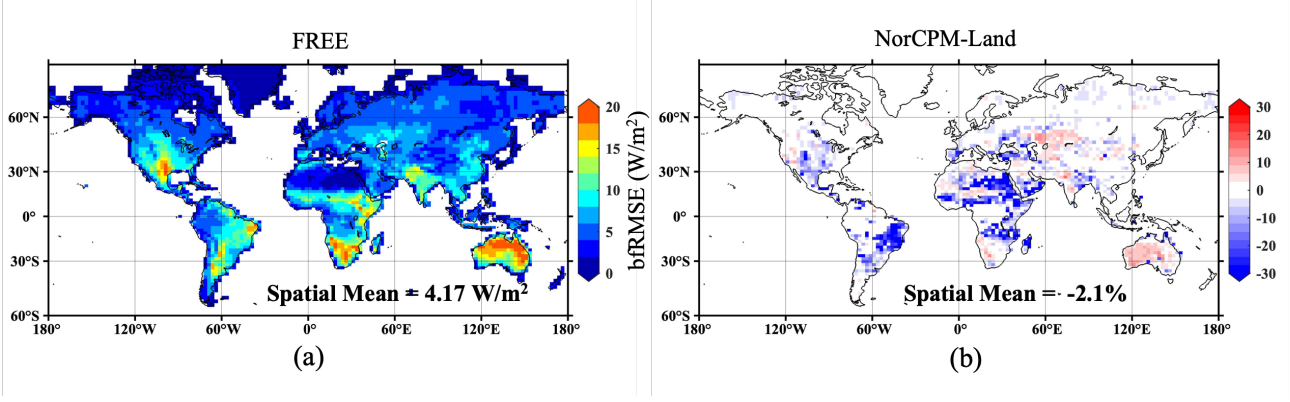

Figure 7. Pointwise bfRMSE of monthly averaged LHF in FREE compared to ERA5-Land (a), and RRMSE in NorCPM-Land – blue color indicates regions with improvement (b).

We further assess the improvement in land-atmosphere feedback by calculating the ACI (Sec. 4, Eq. 10). This analysis is conducted for four seasons: March to May (MAM), June to August (JJA), September to November (SON), and December to February (DJF).

During the MAM season, there is a prolonged precipitation period over East Africa, which exhibits strong coupling with latent heat flux, as shown in ERA5-Land (Fig. 8a). However, in FREE (Fig. 8c) this coupling is absent. The assimilation of SM improves latent heat flux and enhances this coupling (Fig. 8b). Circles highlight some key locations that exhibit improved coupling after SM assimilation. During summer season, high potential evaporation (PET) causes large fluctuation in SM leading to substantial impact on low level atmosphere over tropics.

Similarly, during the JJA season, there is an increased coupling strength observed over India following SM assimilation (Fig. 8e), aligning with the coupling pattern in ERA5-Land (Fig. 8d). Additionally, a strengthening of coupling over the Sahel region (highlighted by a black rectangle) is evident during JJA. During JJA, large values of PET in arid regions results in low persistence in SM. This high variability in SM is synchronised well after SM assimilation in NorCPM-Land, hence has better atmospheric coupling compared to FREE. Other areas with lower PET relative to precipitation experience SM saturation, resulting in little impact on the atmosphere.

https://doi.org/10.5194/gmd-2023-217
Preprint. Discussion started: 4 January 2024

Geoscientific Model Development Discussions

Furthermore, during the SON season, the influence of latent heat flux on precipitation improves over the USA, as observed in Fig. 8g and 8h. A consistent improvement is observed over Australia, particularly during DJF (Fig. 8k and 8j), indicating enhanced land-atmosphere coupling. At high latitudes, weak insolation causes small PET values. Thus,variations in SM have minimal effect on the latent heat flow and, in turn, the atmosphere in this regions during DJF.

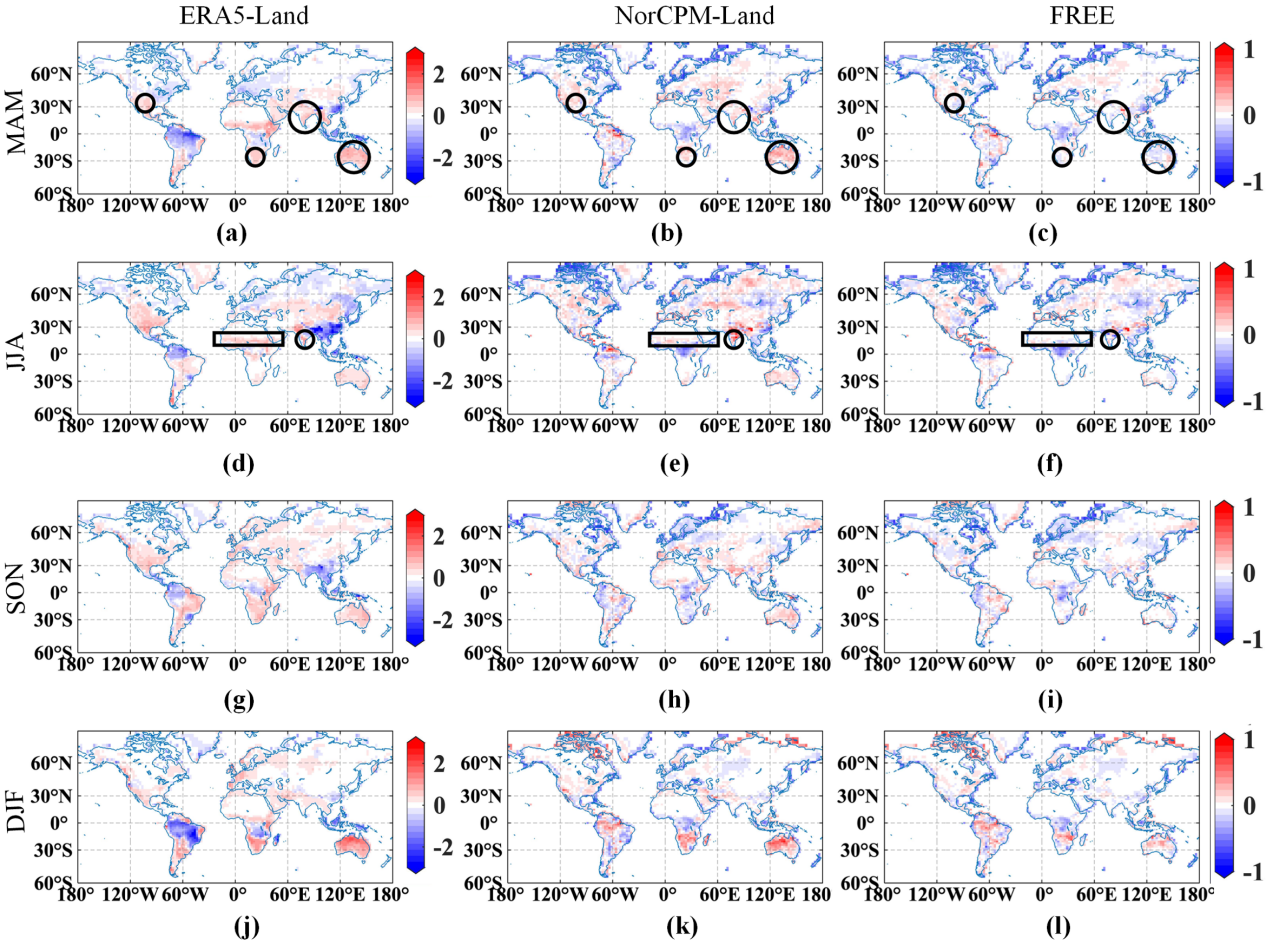

Figure 8. ACI for ERA5-Land (a,d,g,j), NorCPM-Land (b,e,h,k) , and FREE (c,f,i,l) at different seasons. Note that the scales for ERA5-Land and the NorCPM and FREE are different.

5.2 Impact on S2S prediction skill

We now assess the added value of land initialisation on S2S predictions by comparing two sets of hindcasts with and without land initialisation using SM assimilation (Sec. 2.5.1). We assess the hindcast skill for SM, T2M, and precipitation and compare them to ERA5 and ERA5-Land (Sec. 3.2).

https://doi.org/10.5194/gmd-2023-217
Preprint. Discussion started: 4 January 2024

Geoscientific Model Development Discussions
Open Access
EGU

340 The predicted SM from Hind-S (Fig. 9a), exhibits significant error across the entire domain, with a spatial mean of 0.043 m^3/m^3. Improved land initialisation with NorCPM-Land in Hind-S+L significantly reduces SM error in most regions at LM0.5 compared to Hind-S (Fig. 9b). This error reduction is largest over the USA, the Sahel, East Africa, France, India, and Australia, and is more prominent on average over mid-latitudes (Fig. 9c). The benefits of SM initialisation are most pronounced at LM0.5 as shown in the longitudinal mean of RRMSE (Fig. 9c) and LM1.5 (Fig. 9d), but some impact can still be noticed at LM2.5
345 (Fig. 9e). At LM3.5, the impact of land initialisation on SM prediction is minimal, and the RRMSE field is very noisy (Fig. 9f).

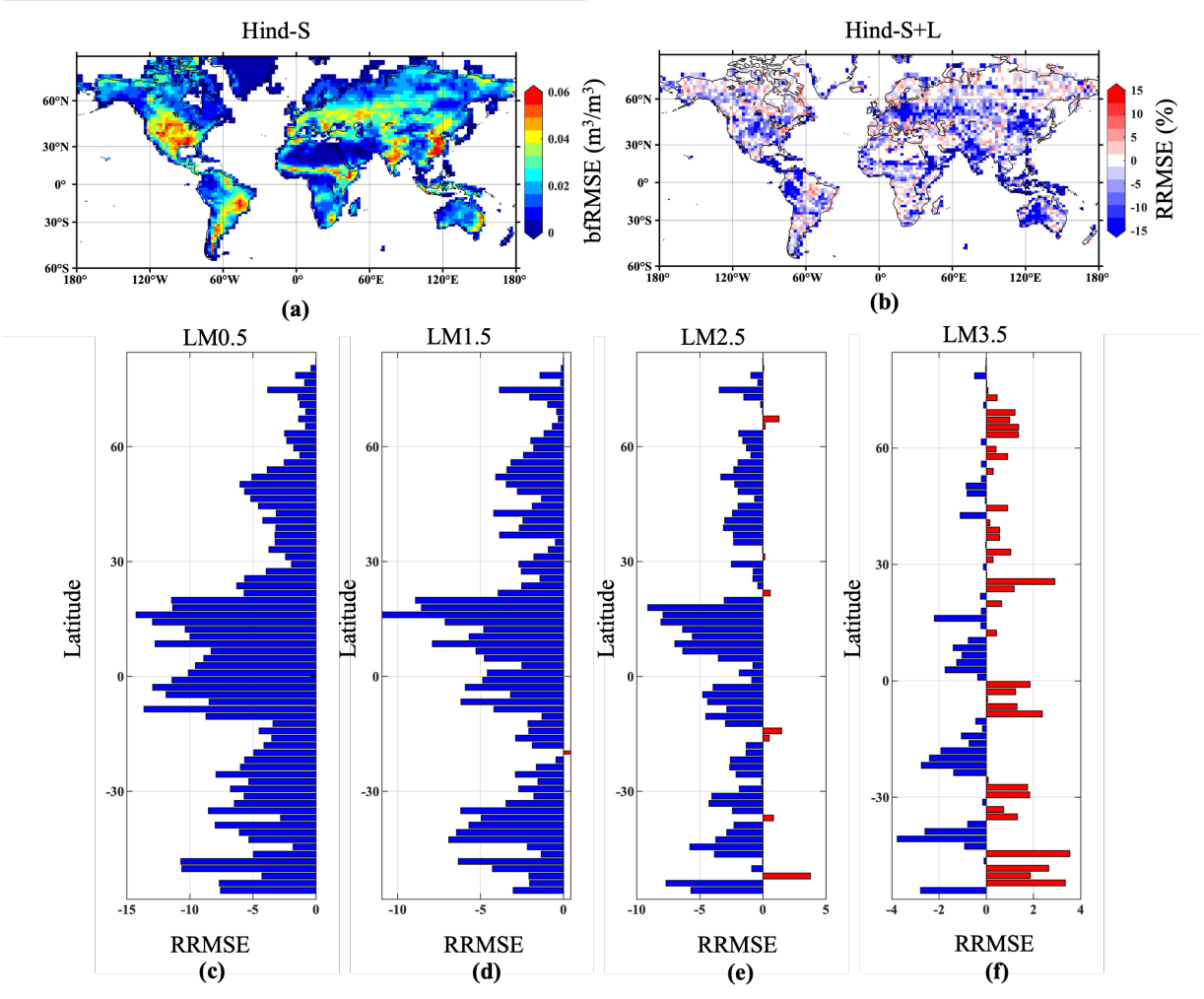

Figure 9. bfRMSE of predicted SM at lead month 0.5 (LM0.5) in Hind-S (a) calculated against ERA5 estimate, and RRMSE in Hind-S+L hindcasts (b). A positive value of RRMSE (blue colour) indicates the percentage reduction of bfRMSE compared to Hind-S. Panels c-d display the Latitude-dependent average of RRMSE in Hind-S+L at LM0.5(c), LM1.5(d), LM2.5(e), and LM3.5(f).

https://doi.org/10.5194/gmd-2023-217
Preprint. Discussion started: 4 January 2024

Geoscientific Model Development Discussions

While NorCPM already demonstrates skill in the tropics under the influence of the El Niño-Southern Oscillation (ENSO) (Wang et al., 2019), the incorporation of NorCPM-Land initialisation clearly enhances its performance. The ACC values in Hind-S+L initialised using NorCPM-Land (Fig. 10b) are considerably higher than in Hind-S (Fig. 10a) at LM0.5, in good agreement with the RRMSE results. The number of points exhibiting a significant positive correlation increase from 452 to 832. However, at longer lead time, the added value of land initialisation diminishes (Fig. 10c). At LM1.5 and LM2.5, the average ACC of SM in Hind-S+L is similar to that of Hind-S.

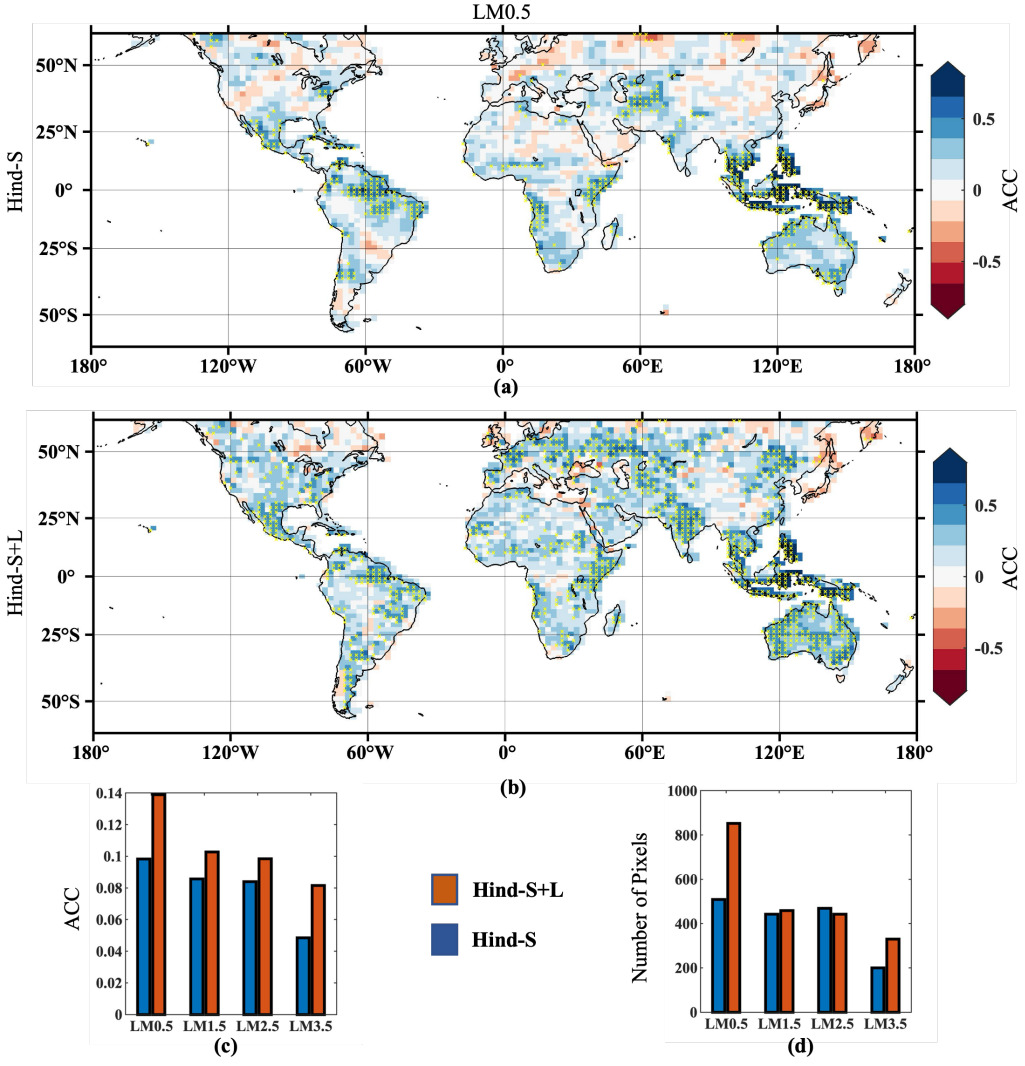

Figure 10. ACC of predicted SM in Hind-S (a) and Hind-S+L (b) at LM0.5 calculated against ERA5-Land. The hatch indicate points having significant ACC. Panel c) shows the spatial mean of ACC at different lead times for the two systems, and panel d) depicts the number of pixels having a significant positive correlation.

https://doi.org/10.5194/gmd-2023-217
Preprint. Discussion started: 4 January 2024

Geoscientific Model Development Discussions

For T2M the bfRMSE of the hindcast from Hind-S (Fig. 11a), is also reduced with NorCPM-Land initialisation in Hind-S+L (Fig. 11b). The error is reduced over land areas in Africa, South America, and India within the tropical band, as a direct response from SM initialisation. Additionally, significant error reduction is observed in Eurasia, Siberia, and Alaska, which can be attributed to strong land-atmospheric couping and teleconnections. For hindcasts initialised in January (Fig. 11c,d), Hind-S shows a 20 % improvement, while for hindcasts initialised in April, July, and October only a 10 % improvement is found.Though we do not assimilate SM in these regions when covered with snow. The assimilation during snow free period can also contribute to this improvement. As during January majority of these regions are covered with snow the major factor for improvement is the atmospheric teleconnections which need further detailed evaluation. In a few regions, a slight increase in error can be observed, which may be related to the imbalance caused by transitioning from an offline simulation (NorCPM-Land) to a fully coupled framework (NorCPM). The impact of land initialisation on T2M beyond LM1.5 is low and noisy.

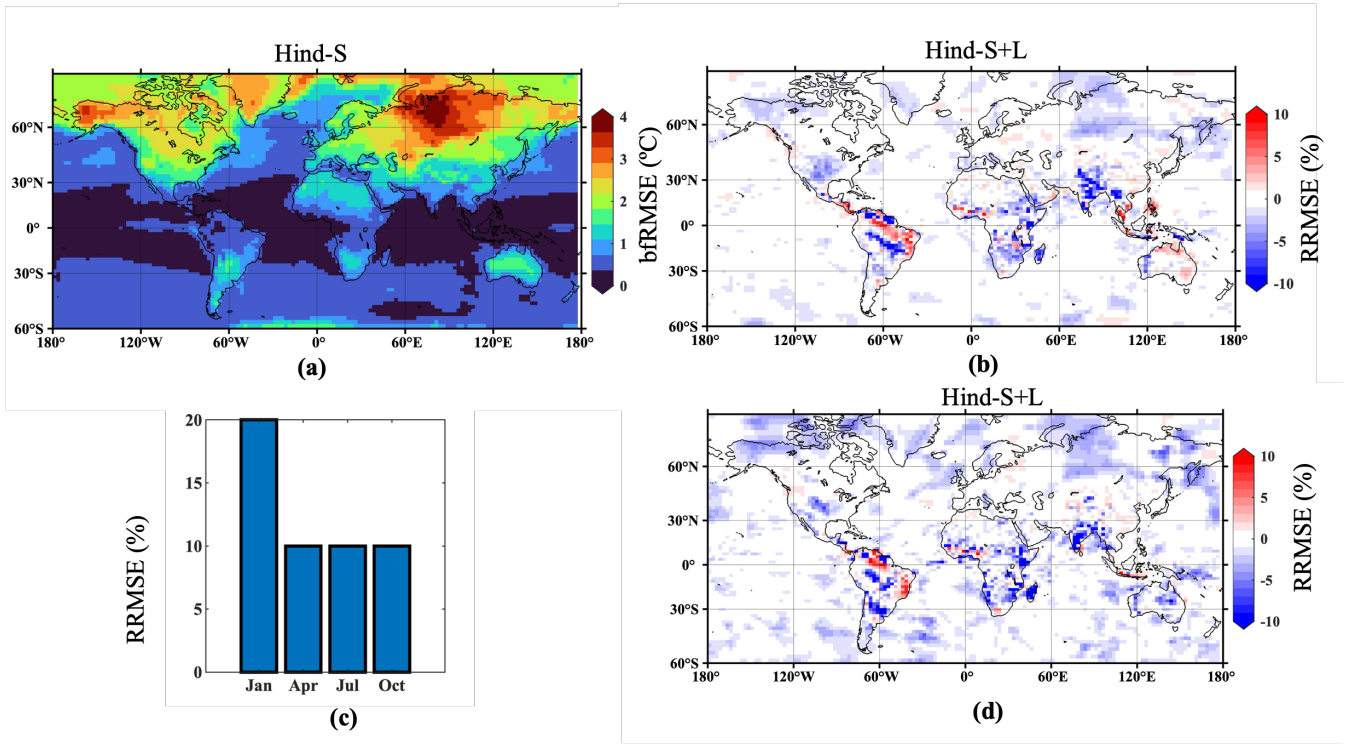

Figure 11. bfRMSE of T2M at LM0.5 in Hind-S calculated against ERA5 (a), the RRMSE of Hind-S+L compared to Hind-S (b), and its average organised by start date (c), the RRMSE of Hind-S+L compared to Hind-S at LM0.5 initialised on January (d) .

We also assess the impact on prediction of temperature extremes. We use the 95th percentile (q95, to classify extreme high T2M) and the 5th percentile (q5, to classify extreme-low T2M) of the hindcast ensemble mean. Hind-S exhibits significant errors in predicting q95 events at LM0.5 over land (Fig. 12 c). This is somewhat mitigated in Hind-S+L (Fig. 12 e). The reduction in q95 error was most pronounced across portions of the United States, Europe, India, Sahel, and parts of Scandinavia (Fig.

https://doi.org/10.5194/gmd-2023-217
Preprint. Discussion started: 4 January 2024

Geoscientific Model Development Discussions

12 e). Similarly, the improved land initialisation helps to reduce error at LM1.5 (Fig. 12 f). The improvement in predicting extreme high temperature can be mainly attributed to drier SM condition in NorCPM-Land that intensifies surface air temperature. These findings suggest that the prevailing SM condition has high importance for the global prediction of extreme high
370 events. Similarly, the Hind-S hindcast exhibits significant errors in predicting q5 at high latitudes, particularly above 30°N, for both LM0.5 and LM1.5 (Fig. 13). However, with land initialisation, the Hind-S+L can better capture q5 in certain areas, such as parts of the Sahel, India, and USA, as well as over eastern Europe, Scandinavia, and much of the United States.

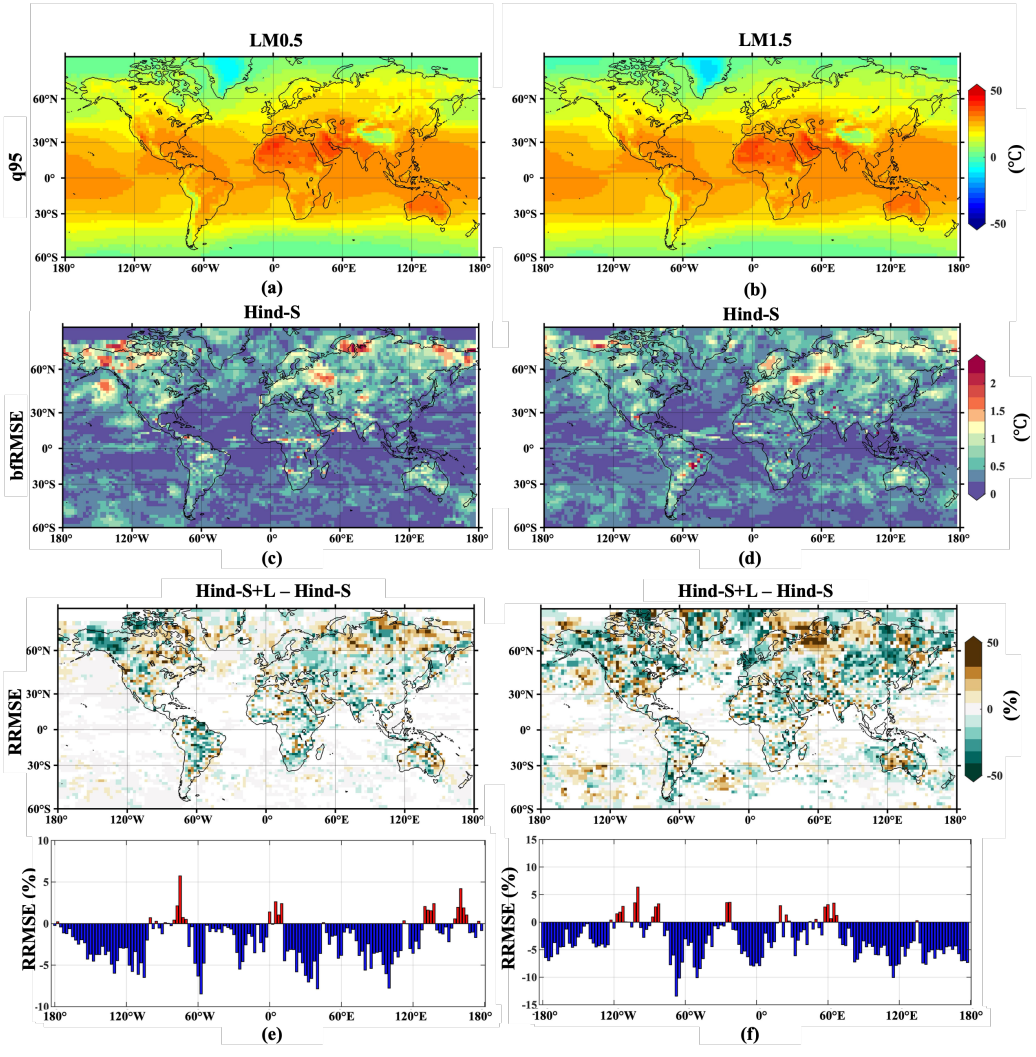

Figure 12. T2M q95 in ERA5 (a,b), bfRMSE of T2M q95 in Hind-S at LM0.5 and LM1.5 with respect to ERA5 (c,d), and RRMSE of T2M q95 in Hind-S+L (e,f).

The bar plots indicate the longitudinal average of RRMSE at corresponding LM.

https://doi.org/10.5194/gmd-2023-217
Preprint. Discussion started: 4 January 2024

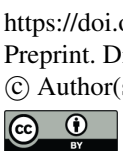

Geoscientific Model Development Discussions

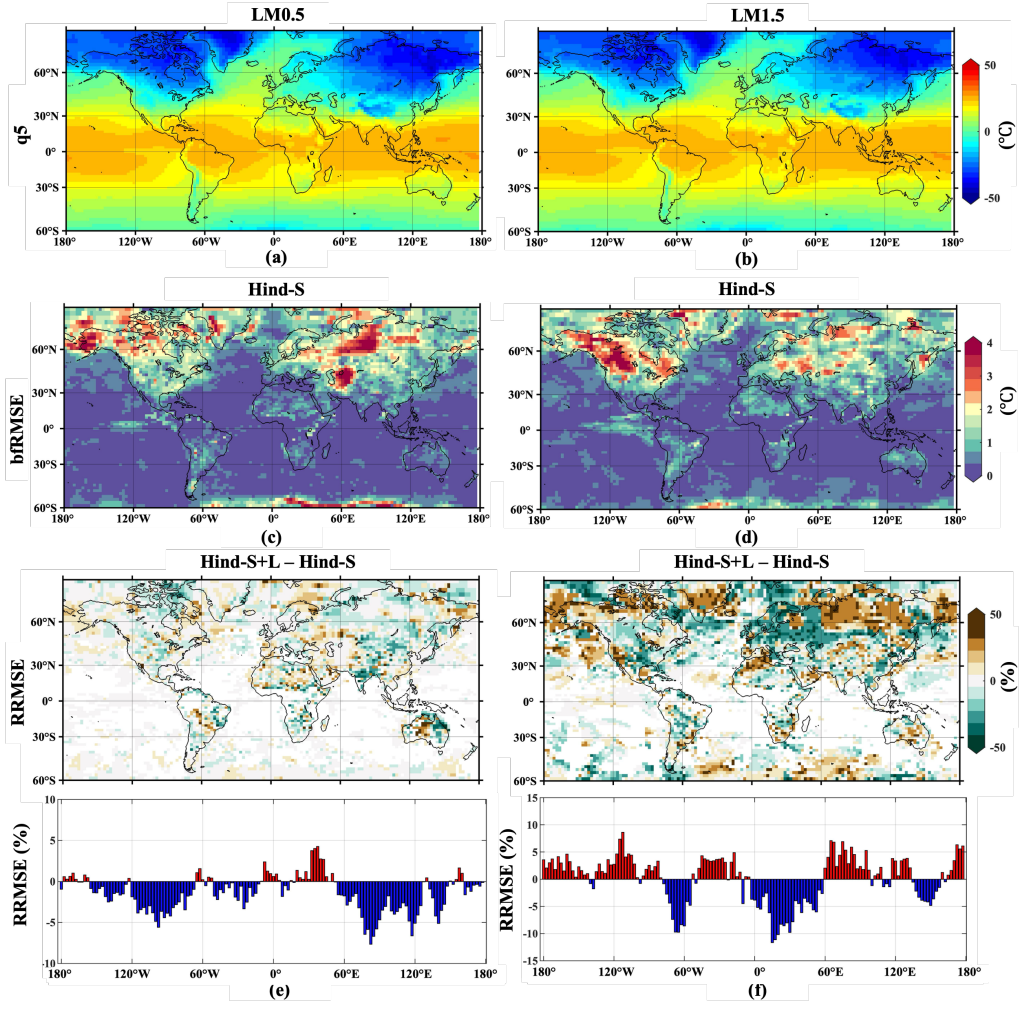

Figure 13. As in Fig. 12 but for q5.

The large error in precipitation in Hind- over equatorial and mid-latitudes at LM0.5 (Fig. 14a) and LM1.5 (Fig. 14b) is reduced over land(Figure 14c) in Hind-S+L. This is particularly notable in regions such as the Sahel, India, and certain areas of the USA during their respective monsoon seasons, in good agreement with previous studies (Koster et al., 2004). The global mean reduction in bfRMSE observed in Hind-S+L is 0.13 mm/day at LM0.5. At LM1.5, while the reduction in Hind-S+L is more sporadic over the ocean, there is still a noticeable improvement over land (Fig. 14d).

https://doi.org/10.5194/gmd-2023-217
Preprint. Discussion started: 4 January 2024

Geoscientific Model Development Discussions

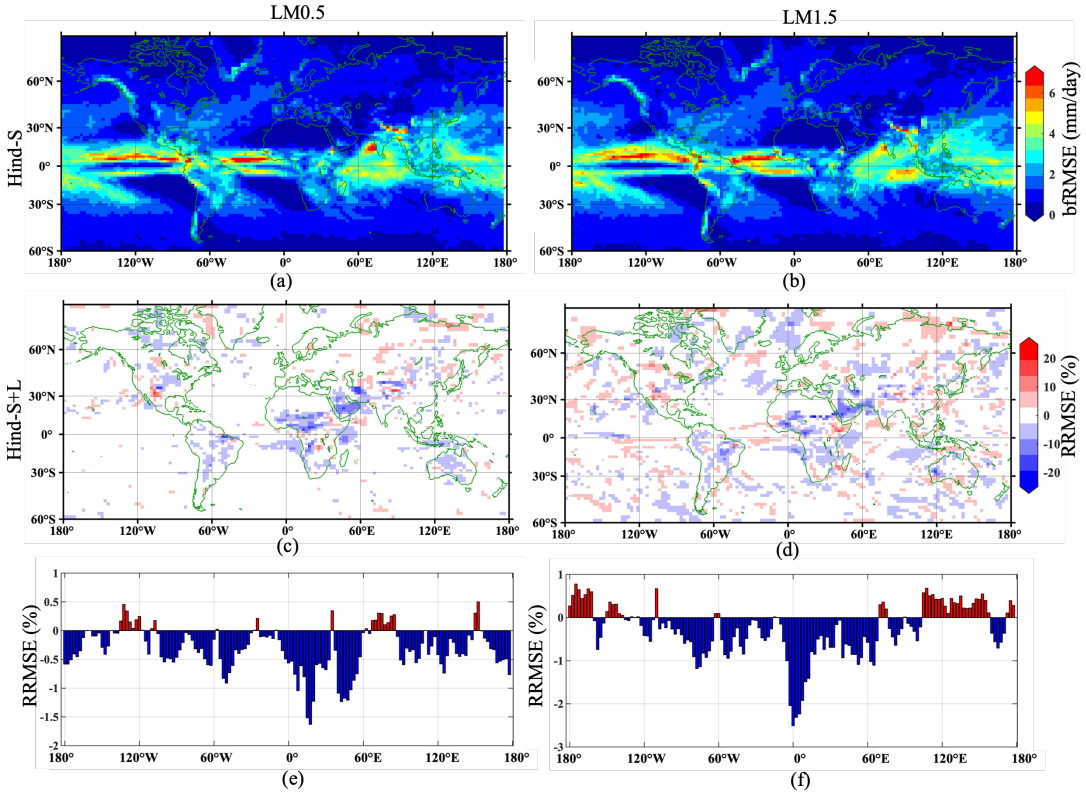

Figure 14. bfRMSE of precipitation with Hind-S at LM0.5 and LM1.5 with respect to ERA5 (a,b) and bfRMSE difference in Hind-S+L (c,d) – where cold colour indicates that error in Hind-S+L are reducing. Bar plots shows the longitude-wise average of RRMSE.

6 Conclusions

In this study, we introduced a framework for developing a land reanalysis tailored to the NorCPM system and to enhance the skill of S2S predictions. We assimilate the daily blended satellite SM data from ESA CCI. The resulting system, NorCPM-Land, operates offline, but utilises fluxes from an ensemble of the same coupled system employed in running the NorCPM climate predictions. This approach enables the generation of an improved land initial state and maintains dynamical compatibility between NorCPM-Land and NorCPM, thus minimising the risk of drift during the prediction. The NorCPM-Land reanalysis span four decades from 1980 to 2019, inclusive.

NorCPM-Land reanalysis demonstrates enhanced capability in capturing the spatiotemporal dynamics of SM. Validation using independent in situ SM data reveals a 10.5 % reduction of error compared to the FREE run. A verification in places where no in situ observation is available were carried against ERA5-Land, and NorCPM-Land reduces the global error by 12.75 % compared to FREE. Improvements were also found in other parameters. NorCPM-Land reduces the error in latent heat flux – particularly at mid-latitudes, such as in USA, Sahel, and India, where strong land-atmosphere coupling exists.

https://doi.org/10.5194/gmd-2023-217
Preprint. Discussion started: 4 January 2024

The NorCPM-Land reanalysis exhibits an overdispersion for SM (meaning that the ensemble spread is larger than the error). It is worth noting that the Free ensemble run is even more over-dispersive. Our bias correction technique – the (CDF) matching – maintains this overdispersion because the CDF function was computed from the FREE run.

In future versions of the system, the fluxes will be provided by a version of NorCPM with constrained atmospheric variability. We expected that the reliability would be improved and that the CDF matching will not maintain the overdispersion of the Free run. Furthermore, we have used a constant inflation factor, which deteriorates the overdispersion. We aim to use adaptive inflation (El Gharamti, 2018), which can inflate or deflate the spread based on reliability statistics.

The hindcast experiments conducted in this study revealed that the added value of land initialisation persists up to a lead time of 2.5 months, with slightly larger benefits observed during the summer and fall seasons. Specifically, at a lead time of 0.5 months, land-surface initialisation positively influences precipitation skill, and to a lesser extent, temperature, aligning with previous research studies (Koster et al., 2004, 2010). This improvement is consistently observed in regions characterised by significant land-atmosphere couplings, such as central India, the central United States, and the Sahel. Although the impact on mean temperature is modest, land surface initialisation enhances the representation of extreme warm and cold temperature events (95^{th} and 5^{th} percentiles) in mid and high latitudes. This improvement is noticeable up to a lead time of 1.5 months, which aligns with the findings of (Van Vuuren et al., 2011) who reported improvements of up to six weeks across Europe. It highlights the importance of capturing pre-existing dry conditions preceding heatwave events to accurately represent their severity. However, it is worth noting that the representation of temperature and precipitation over the ocean is slightly degraded with land initialisation. This may be attributed to the lack of full dynamical agreement between the land initial conditions and the rest of the system in oceanic regions, leading to imbalances that outweigh the benefits of land initialisation. In a future improvement, we aim to directly assimilate SM within our coupled system to address this issue.

The forthcoming research endeavors of NorCPM-Land will center on the integration of real-time satellite SM data sources to enhance the operational capabilities of NorCPM-Land. This is necessitated by the limited operability and considerable latency associated with the current use of the ESA CCI dataset. In the operational version of NorCPM-land the SM observation data will stem from Climate Change Service (C3S), which are produced on a 10-day cycle with 10-day latency. Moreover, the integration will encompass additional land surface variables, including snow and skin temperature, along with enhanced forcing data. These advancements are anticipated to contribute significantly to the enhancement of prediction accuracy, particularly in high-latitude regions.

Code availability. The code of Norwegian Earth System Model (NorESM), Norwegian Climate Prediction Model (NorCPM version1) are available online on the Norwegian Earth System Modeling hub https://github.com/NorESMhub. Specific details about NorCPM can be found in the website https://wiki.app.uib.no/norcpm/index.php/Norwegian_Climate_Prediction_Model.

https://doi.org/10.5194/gmd-2023-217
Preprint. Discussion started: 4 January 2024

Geoscientific Model Development Discussions

Data availability. The ESA CCI merged soil moisture data can be obtained from the climate change initiative website https://www.esa-soilmoisture-cci.org. The reference data from ERA-Land can be obtained from the Copernicus web services https://cds.climate.copernicus.eu/cdsapp#!/dataset/reanalysis-era5-land?tab=form. The insitu soil moisture from International Soil Moisture network can be found at data hosting facility https://ismn.earth/en/. The GLDAS data can be obtained from https://disc.gsfc.nasa.gov/datasets?keywords=GLDAS.

Author contributions. ASN, FC, and NK initiated this research and co-lead the writing of this paper. ASN developed the land data assimilation module for NorCPM, performed all simulations and validation of results. FC supervised the data assimilation setup. ASN wrote the first draft of the manuscript. All authors contributed to improvement of ideas, software, testing, evaluation, writing of paper, and proof reading.

Competing interests. The authors have no competing interest to declare that are relevant to the content of this article.

Acknowledgements. The research was partly funded by Research Council of Norway under the NORKLIMA research programme (EPOCASA; 229774/E10), and the Climate Futures research centre (grant 309562). This work has also received a grant for computer time partly from the Norwegian Program for supercomputing (NOTUR2, project no. NN9039K) and a storage grant (NORSTORE, NS9039K). This work also used high-performance computing and storage resources on the Norwegian infrastructure for computational science: NN9873K and NS9873K

https://doi.org/10.5194/gmd-2023-217
Preprint. Discussion started: 4 January 2024

Geoscientific Model Development Discussions

References

Al-Yaari, A., Dayau, S., Chipeaux, C., Aluome, C., Kruszewski, A., Loustau, D., and Wigneron, J.-P.: The AQUI soil moisture network for satellite microwave remote sensing validation in South-Western France, Remote Sensing, 10, 1839, 2018.

Anderson, J. L.: An ensemble adjustment Kalman filter for data assimilation, Monthly weather review, 129, 2884–2903, 2001.

Assmann, K., Bentsen, M., Segschneider, J., and Heinze, C.: An isopycnic ocean carbon cycle model, Geoscientific Model Development, 3, 143–167, 2010.

Bentsen, M., Bethke, I., Debernard, J. B., Iversen, T., Kirkevåg, A., Seland, Ø., Drange, H., Roelandt, C., Seierstad, I. A., Hoose, C., et al.: The Norwegian Earth System Model, NorESM1-M–Part 1: description and basic evaluation of the physical climate, Geoscientific Model Development, 6, 687–720, 2013.

Bethke, I., Wang, Y., Counillon, F., Keenlyside, N., Kimmritz, M., Fransner, F., Samuelsen, A., Langehaug, H., Svendsen, L., Chiu, P.-G., et al.: NorCPM1 and its contribution to CMIP6 DCPP, Geoscientific Model Development, 14, 7073–7116, 2021.

Bleck, R., Rooth, C., Hu, D., and Smith, L. T.: Salinity-driven thermocline transients in a wind-and thermohaline-forced isopycnic coordinate model of the North Atlantic, Journal of Physical Oceanography, 22, 1486–1505, 1992.

Carrassi, A., Weber, R. J., Guemas, V., Doblas-Reyes, F. J., Asif, M., and Volpi, D.: Full-field and anomaly initialization using a low-order climate model: A comparison and proposals for advanced formulations, Nonlinear Processes in Geophysics, 21, 521–537, https://doi.org/10.5194/npg-21-521-2014, 2014.

Chen, F., Mitchell, K., Schaake, J., Xue, Y., Pan, H.-L., Koren, V., Duan, Q. Y., Ek, M., and Betts, A.: Modeling of land surface evaporation by four schemes and comparison with FIFE observations, Journal of Geophysical Research: Atmospheres, 101, 7251–7268, 1996.

Cosby, B., Hornberger, G., Clapp, R., and Ginn, T.: A statistical exploration of the relationships of soil moisture characteristics to the physical properties of soils, Water resources research, 20, 682–690, 1984.

Counillon, F., Bethke, I., Keenlyside, N., Bentsen, M., Bertino, L., and Zheng, F.: Seasonal-to-decadal predictions with the ensemble Kalman filter and the Norwegian Earth System Model: a twin experiment, Tellus A: Dynamic Meteorology and Oceanography, 66, 21 074, 2014.

Counillon, F., Keenlyside, N., Bethke, I., Wang, Y., Billeau, S., Shen, M. L., and Bentsen, M.: Flow-dependent assimilation of sea surface temperature in isopycnal coordinates with the Norwegian Climate Prediction Model, Tellus A: Dynamic Meteorology and Oceanography, 68, 32 437, 2016.

Dai, Y., Zeng, X., Dickinson, R. E., Baker, I., Bonan, G. B., Bosilovich, M. G., Denning, A. S., Dirmeyer, P. A., Houser, P. R., Niu, G., et al.: The common land model, Bulletin of the American Meteorological Society, 84, 1013–1024, 2003.

De Rosnay, P., Drusch, M., Vasiljevic, D., Balsamo, G., Albergel, C., and Isaksen, L.: A simplified Extended Kalman Filter for the global operational soil moisture analysis at ECMWF, Quarterly Journal of the Royal Meteorological Society, 139, 1199–1213, 2013.

Dente, L., Su, Z., and Wen, J.: Validation of SMOS soil moisture products over the Maqu and Twente regions, Sensors, 12, 9965–9986, 2012.

Dirmeyer, P. A. and Halder, S.: Sensitivity of numerical weather forecasts to initial soil moisture variations in CFSv2, Weather and Forecasting, 31, 1973–1983, 2016.

Dirmeyer, P. A., Halder, S., and Bombardi, R.: On the harvest of predictability from land states in a global forecast model, Journal of Geophysical Research: Atmospheres, 123, 13–111, 2018.

Dorigo, W., Van Oevelen, P., Wagner, W., Drusch, M., Mecklenburg, S., Robock, A., and Jackson, T.: A new international network for in situ soil moisture data, Eos, Transactions American Geophysical Union, 92, 141–142, 2011.

https://doi.org/10.5194/gmd-2023-217
Preprint. Discussion started: 4 January 2024

Drusch, M., Scipal, K., De Rosnay, P., Balsamo, G., Andersson, E., Bougeault, P., and Viterbo, P.: Towards a Kalman Filter based soil moisture analysis system for the operational ECMWF Integrated Forecast System, Geophysical Research Letters, 36, 2009.

El Gharamti, M.: Enhanced adaptive inflation algorithm for ensemble filters, Monthly Weather Review, 146, 623–640, 2018.

Entekhabi, D., Njoku, E. G., O'Neill, P. E., Kellogg, K. H., Crow, W. T., Edelstein, W. N., Entin, J. K., Goodman, S. D., Jackson, T. J., Johnson, J., et al.: The soil moisture active passive (SMAP) mission, Proceedings of the IEEE, 98, 704–716, 2010.

Evensen, G.: The ensemble Kalman filter: Theoretical formulation and practical implementation, Ocean dynamics, 53, 343–367, 2003.

Fischer, E. M., Seneviratne, S. I., Vidale, P. L., Lüthi, D., and Schär, C.: Soil moisture–atmosphere interactions during the 2003 European summer heat wave, Journal of Climate, 20, 5081–5099, 2007.

Fortin, V., Abaza, M., Anctil, F., and Turcotte, R.: Why should ensemble spread match the RMSE of the ensemble mean?, Journal of Hydrometeorology, 15, 1708–1713, 2014.

Gaiser, P. W., St Germain, K. M., Twarog, E. M., Poe, G. A., Purdy, W., Richardson, D., Grossman, W., Jones, W. L., Spencer, D., Golba, G., et al.: The WindSat spaceborne polarimetric microwave radiometer: Sensor description and early orbit performance, IEEE Transactions on Geoscience and Remote Sensing, 42, 2347–2361, 2004.

Gent, P. R., Danabasoglu, G., Donner, L. J., Holland, M. M., Hunke, E. C., Jayne, S. R., Lawrence, D. M., Neale, R. B., Rasch, P. J., Vertenstein, M., et al.: The community climate system model version 4, Journal of climate, 24, 4973–4991, 2011.

González-Zamora, Á., Sánchez, N., Pablos, M., and Martínez-Fernández, J.: CCI soil moisture assessment with SMOS soil moisture and in situ data under different environmental conditions and spatial scales in Spain, Remote Sensing of Environment, 225, 469–482, 2019.

Gruber, A., Scanlon, T., van der Schalie, R., Wagner, W., and Dorigo, W.: Evolution of the ESA CCI Soil Moisture climate data records and their underlying merging methodology, Earth System Science Data, 11, 717–739, 2019.

Guo, Z., Dirmeyer, P. A., and DelSole, T.: Land surface impacts on subseasonal and seasonal predictability, Geophysical Research Letters, 38, 2011.

Hermanson, L., Smith, D., Seabrook, M., Bilbao, R., Doblas-Reyes, F., Tourigny, E., Lapin, V., Kharin, V. V., Merryfield, W. J., Sospedra-Alfonso, R., et al.: WMO global annual to decadal climate update: A prediction for 2021–25, Bulletin of the American Meteorological Society, 103, E1117–E1129, 2022.

Hersbach, H., Bell, B., Berrisford, P., Hirahara, S., Horányi, A., Muñoz-Sabater, J., Nicolas, J., Peubey, C., Radu, R., Schepers, D., et al.: The ERA5 global reanalysis, Quarterly Journal of the Royal Meteorological Society, 146, 1999–2049, 2020.

Holland, M. M., Bailey, D. A., Briegleb, B. P., Light, B., and Hunke, E.: Improved sea ice shortwave radiation physics in CCSM4: The impact of melt ponds and aerosols on Arctic sea ice, Journal of Climate, 25, 1413–1430, 2012.

Hurrell, J. W., Holland, M. M., Gent, P. R., Ghan, S., Kay, J. E., Kushner, P. J., Lamarque, J.-F., Large, W. G., Lawrence, D., Lindsay, K., et al.: The community earth system model: a framework for collaborative research, Bulletin of the American Meteorological Society, 94, 1339–1360, 2013.

Ikonen, J., Smolander, T., Rautiainen, K., Cohen, J., Lemmetyinen, J., Salminen, M., and Pulliainen, J.: Spatially distributed evaluation of ESA CCI Soil Moisture products in a northern boreal forest environment, Geosciences, 8, 51, 2018.

Ines, A. V., Das, N. N., Hansen, J. W., and Njoku, E. G.: Assimilation of remotely sensed soil moisture and vegetation with a crop simulation model for maize yield prediction, Remote Sensing of Environment, 138, 149–164, 2013.

Jensen, K. H. and Refsgaard, J. C.: HOBE: The Danish hydrological observatory, Vadose Zone Journal, 17, 1–24, 2018.

https://doi.org/10.5194/gmd-2023-217
Preprint. Discussion started: 4 January 2024

Karspeck, A. R., Danabasoglu, G., Anderson, J., Karol, S., Collins, N., Vertenstein, M., Raeder, K., Hoar, T., Neale, R., Edwards, J., et al.: A global coupled ensemble data assimilation system using the Community Earth System Model and the Data Assimilation Research Testbed, Quarterly Journal of the Royal Meteorological Society, 144, 2404–2430, 2018.

Kerr, Y. H., Waldteufel, P., Wigneron, J.-P., Delwart, S., Cabot, F., Boutin, J., Escorihuela, M.-J., Font, J., Reul, N., Gruhier, C., et al.: The SMOS mission: New tool for monitoring key elements ofthe global water cycle, Proceedings of the IEEE, 98, 666–687, 2010.

Kimmritz, M., Counillon, F., Smedsrud, L. H., Bethke, I., Keenlyside, N., Ogawa, F., and Wang, Y.: Impact of ocean and sea ice initialisation on seasonal prediction skill in the Arctic, Journal of Advances in Modeling Earth Systems, 11, 4147–4166, 2019.

Kirkevåg, A., Iversen, T., Seland, Ø., Hoose, C., Kristjánsson, J., Struthers, H., Ekman, A. M., Ghan, S., Griesfeller, J., Nilsson, E. D., et al.: Aerosol–climate interactions in the norwegian earth system model–NorESM1-M, Geoscientific Model Development, 6, 207–244, 2013.

Koster, R. D., Suarez, M. J., Ducharne, A., Stieglitz, M., and Kumar, P.: A catchment-based approach to modeling land surface processes in a general circulation model: 1. Model structure, Journal of Geophysical Research: Atmospheres, 105, 24 809–24 822, 2000.

Koster, R. D., Dirmeyer, P. A., Guo, Z., Bonan, G., Chan, E., Cox, P., Gordon, C., Kanae, S., Kowalczyk, E., Lawrence, D., et al.: Regions of strong coupling between soil moisture and precipitation, Science, 305, 1138–1140, 2004.

Koster, R. D., Mahanama, S., Yamada, T., Balsamo, G., Berg, A., Boisserie, M., Dirmeyer, P., Doblas-Reyes, F., Drewitt, G., Gordon, C., et al.: Contribution of land surface initialization to subseasonal forecast skill: First results from a multi-model experiment, Geophysical Research Letters, 37, 2010.

Kumar, S. V., Reichle, R. H., Harrison, K. W., Peters-Lidard, C. D., Yatheendradas, S., and Santanello, J. A.: A comparison of methods for a priori bias correction in soil moisture data assimilation, Water Resources Research, 48, 2012.

Larson, K. M., Small, E. E., Gutmann, E. D., Bilich, A. L., Braun, J. J., and Zavorotny, V. U.: Use of GPS receivers as a soil moisture network for water cycle studies, Geophysical Research Letters, 35, 2008.

Lawrence, D. M. and Slater, A. G.: Incorporating organic soil into a global climate model, Climate Dynamics, 30, 145–160, 2008.

Lawrence, D. M., Oleson, K. W., Flanner, M. G., Thornton, P. E., Swenson, S. C., Lawrence, P. J., Zeng, X., Yang, Z.-L., Levis, S., Sakaguchi, K., et al.: Parameterization improvements and functional and structural advances in version 4 of the Community Land Model, Journal of Advances in Modeling Earth Systems, 3, 2011.

Li, F., Orsolini, Y., Keenlyside, N., Shen, M.-L., Counillon, F., and Wang, Y.: Impact of snow initialization in subseasonal-to-seasonal winter forecasts with the Norwegian Climate Prediction Model, Journal of Geophysical Research: Atmospheres, 124, 10 033–10 048, 2019.

Liang, X., Lettenmaier, D. P., Wood, E. F., and Burges, S. J.: A simple hydrologically based model of land surface water and energy fluxes for general circulation models, Journal of Geophysical Research: Atmospheres, 99, 14 415–14 428, 1994.

Magnusson, L., Alonso-Balmaseda, M., Corti, S., Molteni, F., and Stockdale, T.: Evaluation of forecast strategies for seasonal and decadal forecasts in presence of systematic model errors, Climate Dynamics, 41, 2393–2409, https://doi.org/10.1007/s00382-012-1599-2, 2013.

Mariotti, A., Ruti, P. M., and Rixen, M.: Progress in subseasonal to seasonal prediction through a joint weather and climate community effort, Npj Climate and Atmospheric Science, 1, 4, 2018.

McColl, K. A., Alemohammad, S. H., Akbar, R., Konings, A. G., Yueh, S., and Entekhabi, D.: The global distribution and dynamics of surface soil moisture, Nature Geoscience, 10, 100–104, 2017.

Meehl, G. A., Richter, J. H., Teng, H., Capotondi, A., Cobb, K., Doblas-Reyes, F., Donat, M. G., England, M. H., Fyfe, J. C., Han, W., et al.: Initialized Earth System prediction from subseasonal to decadal timescales, Nature Reviews Earth & Environment, 2, 340–357, 2021.

https://doi.org/10.5194/gmd-2023-217
Preprint. Discussion started: 4 January 2024

Merryfield, W. J., Baehr, J., Batté, L., Becker, E. J., Butler, A. H., Coelho, C. A., Danabasoglu, G., Dirmeyer, P. A., Doblas-Reyes, F. J., Domeisen, D. I., et al.: Current and emerging developments in subseasonal to decadal prediction, Bulletin of the American Meteorological Society, 101, E869–E896, 2020.

Müller, O. V., Vidale, P. L., Vannière, B., Schiemann, R., Senan, R., Haarsma, R. J., and Jungclaus, J. H.: Land–atmosphere coupling sensitivity to GCMs resolution: A multimodel assessment of local and remote processes in the Sahel hot spot, Journal of Climate, 34, 967–985, 2021.

Muñoz-Sabater, J., Dutra, E., Agustí-Panareda, A., Albergel, C., Arduini, G., Balsamo, G., Boussetta, S., Choulga, M., Harrigan, S., Hersbach, H., et al.: ERA5-Land: A state-of-the-art global reanalysis dataset for land applications, Earth System Science Data, 13, 4349–4383, 2021.

Nair, A. S. and Indu, J.: Enhancing Noah land surface model prediction skill over Indian subcontinent by assimilating SMOPS blended soil moisture, Remote Sensing, 8, 976, 2016.

Nair, A. S. and Indu, J.: Improvement of land surface model simulations over India via data assimilation of satellite-based soil moisture products, Journal of Hydrology, 573, 406–421, 2019.

Nair, A. S., Mangla, R., and Indu, J.: Remote sensing data assimilation, Hydrological Sciences Journal, 67, 2457–2489, 2022.

Njoku, E. G., Jackson, T. J., Lakshmi, V., Chan, T. K., and Nghiem, S. V.: Soil moisture retrieval from AMSR-E, IEEE transactions on Geoscience and remote sensing, 41, 215–229, 2003.

Oleson, K., Lawrence, D., Bonan, G., Drewniak, B., Huang, M., Koven, C., Levis, S., Li, F., Riley, W., Subin, Z., et al.: Technical description of version 4.5 of the Community Land Model (CLM), NCAR Tech, Notes (NCAR/TN-478+ STR), 605, 2010.

Orth, R. and Seneviratne, S. I.: Analysis of soil moisture memory from observations in Europe, Journal of Geophysical Research: Atmospheres, 117, 2012.

Pohlmann, H., Jungclaus, J. H., Köhl, A., Stammer, D., and Marotzke, J.: Initializing decadal climate predictions with the GECCO oceanic synthesis: Effects on the North Atlantic, Journal of Climate, 22, 3926–3938, 2009.

Pradhan, A., Nair, A. S., Indu, J., Makarieva, O., and Nesterova, N.: Leveraging Soil Moisture Assimilation in Permafrost Affected Regions, Remote Sensing, 15, 1532, 2023.

Reichle, R. H. and Koster, R. D.: Bias reduction in short records of satellite soil moisture, Geophysical Research Letters, 31, 2004.

Rodell, M., Houser, P., Jambor, U., Gottschalck, J., Mitchell, K., Meng, C.-J., Arsenault, K., Cosgrove, B., Radakovich, J., Bosilovich, M., et al.: The global land data assimilation system, Bulletin of the American Meteorological society, 85, 381–394, 2004.

Rodwell, M., Lang, S., Ingleby, N., Bormann, N., Hólm, E., Rabier, F., Richardson, D., and Yamaguchi, M.: Reliability in ensemble data assimilation, Quarterly Journal of the Royal Meteorological Society, 142, 443–454, 2016.

Santanello Jr, J. A., Dirmeyer, P. A., Ferguson, C. R., Findell, K. L., Tawfik, A. B., Berg, A., Ek, M., Gentine, P., Guillod, B. P., Van Heerwaarden, C., et al.: Land–atmosphere interactions: The LoCo perspective, Bulletin of the American Meteorological Society, 99, 1253–1272, 2018.

Schaefer, G. L., Cosh, M. H., and Jackson, T. J.: The USDA natural resources conservation service soil climate analysis network (SCAN), Journal of Atmospheric and Oceanic Technology, 24, 2073–2077, 2007.

Scipal, K., Drusch, M., and Wagner, W.: Assimilation of a ERS scatterometer derived soil moisture index in the ECMWF numerical weather prediction system, Advances in water resources, 31, 1101–1112, 2008.

Seneviratne, S. I., Corti, T., Davin, E. L., Hirschi, M., Jaeger, E. B., Lehner, I., Orlowsky, B., and Teuling, A. J.: Investigating soil moisture–climate interactions in a changing climate: A review, Earth-Science Reviews, 99, 125–161, 2010.

https://doi.org/10.5194/gmd-2023-217
Preprint. Discussion started: 4 January 2024

Seo, E., Lee, M.-I., Jeong, J.-H., Koster, R. D., Schubert, S. D., Kim, H.-M., Kim, D., Kang, H.-S., Kim, H.-K., MacLachlan, C., et al.: Impact of soil moisture initialization on boreal summer subseasonal forecasts: mid-latitude surface air temperature and heat wave events, Climate dynamics, 52, 1695–1709, 2019.

Seo, E., Lee, M.-I., Schubert, S. D., Koster, R. D., and Kang, H.-S.: Investigation of the 2016 Eurasia heat wave as an event of the recent warming, Environmental Research Letters, 15, 114 018, 2020.

Smith, A. B., Walker, J. P., Western, A. W., Young, R., Ellett, K., Pipunic, R., Grayson, R., Siriwardena, L., Chiew, F. H., and Richter, H.: The Murrumbidgee soil moisture monitoring network data set, Water Resources Research, 48, 2012.

Talagrand, O.: 4D-VAR: four-dimensional variational assimilation, Advanced Data Assimilation for Geosciences: Lecture Notes of the Les Houches School of Physics: Special Issue, p. 1, 2014.

Taylor, C. M., de Jeu, R. A., Guichard, F., Harris, P. P., and Dorigo, W. A.: Afternoon rain more likely over drier soils, Nature, 489, 423–426, 2012a.

Taylor, K. E., Stouffer, R. J., and Meehl, G. A.: An overview of CMIP5 and the experiment design, Bulletin of the American meteorological Society, 93, 485–498, 2012b.

Tjiputra, J., Roelandt, C., Bentsen, M., Lawrence, D., Lorentzen, T., Schwinger, J., Seland, Ø., and Heinze, C.: Evaluation of the carbon cycle components in the Norwegian Earth System Model (NorESM), Geoscientific Model Development Discussions, 5, 3035–3087, 2012.

Ulaby, F., Moore, R., and Fung, A.: Microwave remote sensing active and passive. radar remote sensing, Surf Scatt Emiss Theory, 2, 819–833, 1987.

Ulaby, F. T., Moore, R. K., and Fung, A. K.: Microwave Remote Sensing Active and Passive-Volume III: From Theory to Applications, MA:Artech House, 1986.

Van Vuuren, D. P., Edmonds, J., Kainuma, M., Riahi, K., Thomson, A., Hibbard, K., Hurtt, G. C., Kram, T., Krey, V., Lamarque, J.-F., et al.: The representative concentration pathways: an overview, Climatic change, 109, 5–31, 2011.

Wagner, W., Hahn, S., Kidd, R., Melzer, T., Bartalis, Z., Hasenauer, S., Figa, J., De Rosnay, P., Jann, A., Schneider, S., et al.: The ASCAT soil moisture product: a review of its, Meteorol. Zeitschrift, 22, 1–29, 2013.

Wang, Y., Counillon, F., Keenlyside, N., Svendsen, L., Gleixner, S., Kimmritz, M., Dai, P., and Gao, Y.: Seasonal predictions initialised by assimilating sea surface temperature observations with the EnKF, Climate Dynamics, 53, 5777–5797, 2019.

Whitaker, J. S. and Hamill, T. M.: Ensemble data assimilation without perturbed observations, Monthly weather review, 130, 1913–1924, 2002.

Yang, K., Qin, J., Zhao, L., Chen, Y., Tang, W., Han, M., Chen, Z., Lv, N., Ding, B., Wu, H., et al.: A multiscale soil moisture and freeze–thaw monitoring network on the third pole, Bulletin of the American Meteorological Society, 94, 1907–1916, 2013.

Young, R., Walker, J., Yeoh, N., Smith, A., Ellett, K., Merlin, O., and Western, A.: Soil moisture and meteorological observations from the Murrumbidgee catchment, Department of Civil and Environmental Engineering, The University of Melbourne, 2008.

Zreda, M., Shuttleworth, W., Zeng, X., Zweck, C., Desilets, D., Franz, T., and Rosolem, R.: COSMOS: The cosmic-ray soil moisture observing system, Hydrology and Earth System Sciences, 16, 4079–4099, 2012.